Cretaceous Research 179 (2026) 106246

Contents lists available at ScienceDirect

Cretaceous Research

journal homepage: www.elsevier.com/locate/CretRes

# Paleoclimate variation during the Cretaceous revealed by geochemical and mineralogical analyses from continental sediments in northern Vietnam

Pham Thi Nga [a], Taro Higuchi [b,c], Kentaro Oe [a], Nguyen Quoc Dinh [d,e], Rajat Mazumder [f,g], Tohru Ohta [h,*]

[a] Graduate School of Creative Sciences and Engineering, Waseda University, 3-4-1 Ookubo, Shinjuku, Tokyo, 169-8555, Japan
[b] Department of Earth Sciences, School of Education, Waseda University, 1-6-1 Nishiwaseda, Shinjuku, Tokyo, 169-8050, Japan
[c] Atmosphere and Ocean Research Institute, the University of Tokyo, 5-1-5, Kashiwanoha, Kashiwa, Chiba, 277-8564, Japan
[d] External Engagement Office, Phenikaa University, Hanoi, 12116, Viet Nam
[e] Environmental Chemistry and Ecotoxicology LAB, Phenikaa University, Hanoi, 12116, Viet Nam
[f] Department of Applied Geosciences, German University of Technology in Oman, Athaibah PC 130, Sultanate of Oman
[g] School of Natural Science and Engineering, National Institute of Advanced Studies, Indian Institute of Science Campus, Bangalore, 560012, India
[h] Department of Earth Sciences, Faculty of Education and Integrated Arts and Sciences, Waseda University, 1-6-1 Nishiwaseda, Shinjuku, Tokyo, 169-8050, Japan

ARTICLE INFO

*Article history:*
Received 23 April 2024
Received in revised form
17 September 2025
Accepted in revised form 17 September 2025
Available online 20 September 2025

*Keywords:*
Paleoclimate
Hinterland weathering
Cretaceous
Southeast Asia
Vietnam

ABSTRACT

Severe aridification has been recognized in low-latitude areas of Southeast Asia during the mid-Cretaceous; however, previous studies mainly focused on continental interior basins. Here, we investigate Cretaceous continental sediments from northern Vietnam, located in the Southeast Asian continental margin, where a precise study has not been conducted. The geochemical and mineralogical characteristics of mudstones collected from the Ban Hang and Yen Chau formations revealed fluctuations in climate conditions in northern Vietnam, including a slight humidification from the Early to mid-Cretaceous and aridification in the Late Cretaceous. Northern Vietnam is considered to have experienced a temperate semi-arid climate in the Early Cretaceous but shifted to a hot and sub-humid environment in the mid-Cretaceous and then returned to arid conditions in the late Period. The results indicate that the coastal area of Southeast Asia was more humid than the inland due to its proximity to the proto-Pacific Ocean. We also detected an increase in humidity in the coastal area during the mid-Cretaceous, contrasting with the inland regions where extreme aridification progressed. This contrasting paleoclimate regime was probably established by the isolation of coastal and inland areas by the tectonic re-configuration of the Southeast Asian continent. During the Cretaceous, closure of the Meso-Tethys Ocean and collisional tectonics generated a coastal mountain range, which caused the orogenic rain-shadow effects, i.e., increased precipitation in the coastal area and intensified desertification in the inland area. The present contribution indicates that the Cretaceous paleoclimate conditions in Southeast Asia were primarily constrained by the regional geographical background rather than the global climate system.


## 1. Introduction

The Cretaceous Period, with its high temperature and atmospheric $CO_2$ concentration (e.g., Retallack, 2001; Royer et al., 2001), is a crucially important subject in paleoclimate studies because it may provide a reference for modern and future climates with greenhouse conditions. Previous studies have revealed significant changes in Earth's atmosphere, hydrosphere, and biosphere during the Cretaceous including the expansion and contraction of atmospheric Hadley circulation (Hasegawa et al., 2012; Hay and Floegel, 2012; Wagner et al., 2013), major ocean anoxic events (Wang et al., 2009; Hu et al., 2012), and the reversal of the oceanic

* Corresponding author.
*E-mail addresses:* phamthinga@toki.waseda.jp (P.T. Nga), taroutokotarou@akane.waseda.jp, taro-h@aori.u-tokyo.ac.jp (T. Higuchi), ken.503484@gmail.com (K. Oe), dinh.nguyenquoc@phenikaa-uni.edu.vn (N.Q. Dinh), rajat.mazumder@gutech.edu.om (R. Mazumder), tohta@waseda.jp (T. Ohta).

https://doi.org/10.1016/j.cretres.2025.106246

thermohaline circulation (see Hay and Floegel, 2012). However, ideas on the potential cause-and-effect of climate change during the Cretaceous should be tested and elucidated on a regional scale as well as on the whole Earth.

The mid-Cretaceous, particularly the Cenomanian–Turonian interval, was the time of the warmest climate and highest atmospheric $CO_2$ concentration during the Cretaceous (e.g., Huber et al., 2002; Wang et al., 2014). Many geological studies have examined the paleoclimate changes of the Southeast Asian continent during the mid-Cretaceous. These studies revealed that the Southeast Asian continent suffered from an extremely arid climate during the mid-Cretaceous as evidenced by the common occurrence of aeolian sandstone and evaporite-bearing sediments (Hasegawa et al., 2010, 2012; Wu et al., 2017; Li G. et al., 2018). The causes of the water cycle change in the mid-Cretaceous region are controversial in several studies. From the distributions of climate-sensitive sediments and paleo-wind direction reconstructions, Hasegawa et al. (2012) suggested that this paleoclimatic change can be explained under the hypothesis that the subtropical high shifted southward due to the shrinking of the Hadley circulation during the mid-Cretaceous. Additionally, Higuchi et al. (2021) utilized an atmospheric-ocean fully coupled model simulator and found that aridification was due to a decrease in precipitation caused by the weakening of atmospheric circulation during high $CO_2$ concentration and global warming. On the other hand, several studies have highlighted the significance of paleogeographical changes in altering the water cycle in Southeast Asia. These changes include shifts in continental distribution and uplift (Farnsworth et al., 2019), as well as the formation of the local coastal mountains (e.g., Wu et al., 2017; Li G. et al., 2018).

Numerous studies have been conducted to reconstruct the Cretaceous paleoclimate in Southeast Asia, but they have primarily focused on the inland basins in South China and the central Indochina Peninsula. The coastal areas of the Asian continental margin and equatorial region have not been precisely investigated. Despite this, climate modelling studies pointed out the importance of the coastal areas in unraveling the paleoclimate of Southeast Asia due to the formation of coastal mountains during the Cretaceous (Zhang et al., 2021a, b). Vietnam is located at the southeastern margin of the Asian continent and can be considered an interesting geological object for interpreting the climate hypothesis. However, there has not been a direct and detailed study of the Vietnamese climate in the Cretaceous until now. In this study, the Cretaceous climate conditions of northern Vietnam are clarified based on geochemical records and mineralogical data from continental redbeds, which are considered essential indicators for paleoclimate reconstruction of the sedimentary basin. The source-rock composition and diagenetic effects are also examined to interpret the paleoclimate by unravelling the extent of hinterland weathering. Particularly, geochemical weathering indices and clay-mineral compositions are utilized, as are commonly used in paleoclimate reconstructions (Ruffell et al., 2002; Baioumy, 2004; Yan et al., 2007; Ohta et al., 2011; Perri and Ohta, 2014; Li et al., 2016).

## 2. Geological setting

### 2.1. Position of northern Vietnam in the Cretaceous Period

Southeast Asia comprises several amalgamated continental fragments derived from Gondwana or Cathaysia that collided during the Paleozoic to Cenozoic (e.g., Metcalfe, 1988, 2002; Hall, 2002). The main tectonic framework of Southeast Asia consists of the South China, Indochina, South Indochina, Thai-Malay, Sibumasu and SW Borneo blocks (Fig. 1), which are bounded by suture zones composed of ophiolites, accretionary complexes, and marine to terrestrial sediments. These blocks generally migrated northward, and accretion to the central Asian continent was completed around the Triassic (Li et al., 2004; Metcalfe, 2011). Since then, the configuration of present-day southwest Asia has already been established in Cretaceous (Hall, 2002; Li et al., 2004; Metcalfe, 2011).

During the Cenozoic, tectonic re-alignments of continental blocks occurred due to the collision of India and Eurasia (e.g., Replumaz and Tapponnier, 2003). This resulted in the extrusion tectonics and the Indochina, South Indochina, Thai-Malay, and Sibumasu blocks, which were displaced southward for more than 1000 km, relative to the South China Block (Yang and Besse, 1993; Sato et al., 1999). These collisions significantly influenced the structural deformations in northern Vietnam and formed many

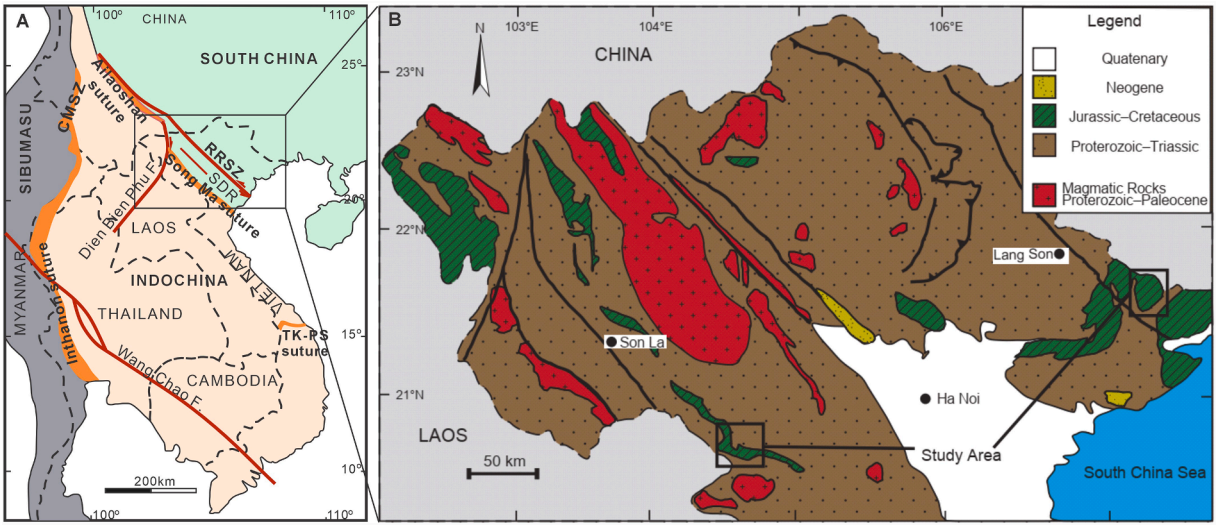


**Fig. 1.** (A) Simplified tectonic map showing boundaries between major tectonic blocks in Southeast Asian mainland (after Shi et al., 2015; Wang et al., 2016). CMSZ = Changning–Menglian Suture Zone; RRSZ = Red River Shear Zone; TK-PS = Tam Ky-Phuoc Son; SDR = Song Da Rift. (B) Geological sketch map of northern Vietnam (after Roger et al., 2012).

different geological structures such as Song Ma suture zone, Song Da rift, and Red River shear zone (Faure et al., 2014; Su et al., 2018, Thanh et al., 2019, Fig. 1A).

As for the northern Vietnam region, Su et al. (2018) studied the crustal structure and revealed that the Song Ma Fault System is the demarcation suture zone between the South China and Indochina blocks (Fig. 1). Therefore, the northeastern region of northern Vietnam including Red River shear zone and Song Da rift belongs to the South China Block.

The Song Ma suture zone that strikes NW-SE is thought to be the convergent boundary between the Indochina block and the South China block (Findlay and Trinh, 1997; Wang et al., 2016; Su et al., 2018). The northeastern region of northern Vietnam, which is part of the South China block, is believed to have remained stable since the Cretaceous. Meanwhile, the rest of Vietnam's territory, from the Song Ma Fault southwards, belongs to the Indochina block and has likely experienced significant latitudinal displacement along the Red River shear zone (Shi et al., 2015; Thanh et al., 2019; Hung et al., 2022). In fact, paleomagnetic records of the studied Cretaceous strata (Yen Chau Formation) show no displacement and rotation since the Cretaceous (Takemoto et al., 2005). Thus, in the Cretaceous, northern Vietnam was situated around 20°N–25°N latitude as in present.

### 2.2. Cretaceous formations

Jurassic–Cretaceous sediments are distributed widely around northern Vietnam including Jurassic continental red beds (Ha Coi and Nam Po formations), Upper Jurassic–Lower Cretaceous volcano-sedimentary beds (Tam Lung and Tu Le formations), and Cretaceous continental red beds (Ban Hang, Yen Chau, and Nam Ma formations) (Thanh and Khuc, 2006; Hung, 2009). The non-marine Cretaceous formations are separately distributed in northern Vietnam including Ban Hang Formation in the northeastern area, Nam Ma Formation in the Muong Te zone, and Yen Chau Formation in the northwestern region. In this study, we collected continental red sediments distributed in Lang Son and Son La provinces described as Ban Hang and Yen Chau formations, respectively (Fig. 1B).

The Ban Hang Formation occurs in the An Chau Synclinorium, which is located along the border with PR China. Outcrops of the Ban Hang Formation can be found in the Ban Hang, Tien Phi, Ban Tam, and Dinh Lap areas. We chose the Dinh Lap area as the study site because the whole sequence of the Ban Hang Formation can be investigated in this area. The Ban Hang Formation is composed mainly of cross-bedded and polymictic conglomerates, sandstone, and reddish-brown to greyish-blue mudstone intercalated with thick-bedded reddish sandstone (Figs. 2A and 2B). The

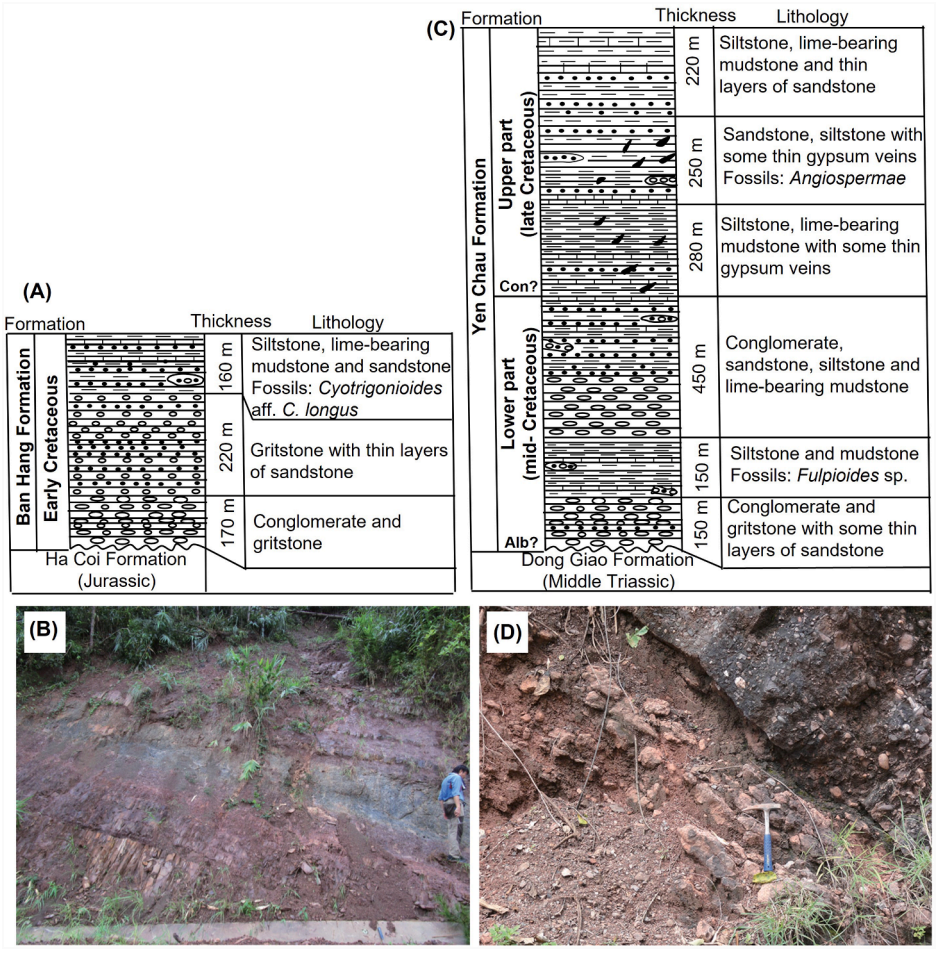


**Fig. 2.** Lithology and representative outcrop photographs of studied formations. (A) Schematic lithostratigraphic column of Ban Hang Formation following Thanh and Khuc (2006); (B) Reddish-brown and grayish-blue mudstones in Ban Hang Formation. (C) Schematic lithostratigraphic column of Yen Chau Formation after Huu et al. (2008). Alb? = Albian, Con? = Coniacian?; (D) Reddish-brown siltstones composed of nodular to tabular carbonate concretions and overlying pebbly sandstone in Yen Chau Formation.

sedimentary facies characteristics indicate that the Ban Hang Formation was deposited in a lacustrine environment (Thanh and Khuc, 2006).

The Ban Hang Formation's depositional age was formerly described as undifferentiated Cretaceous based on its unconformable position upon the Jurassic terrigenous red beds of the Ha Coi Formation. However, fresh-to-brackish-water bivalve fossils collected from mudstone layers of the formation were determined to be *Cyotrigonioides* aff. *C. longus*, which indicates an Early Cretaceous age (Khien, 2005; Thanh and Khuc, 2006). The lower age limit of the Ban Hang Formation is uncertain, however, the Ban Hang Formation unconformably overlies the Jurassic terrigenous red beds of the Ha Coi Formation (Thanh and Khuc, 2006), suggesting the Early Cretaceous age.

The Yen Chau Formation occurs widely in the western part of northern Vietnam as discontinuous large bands in Son La, Lai Chau, and Hoa Binh provinces (Thanh and Khuc, 2006). In this study, the red bed samples were collected from Yen Chau valley which was described as the lectostratotype section of the Yen Chau Formation (Fig. 1B). In this area, the formation, which has a thickness of 1500 m, is divided into two parts. The lower part is composed mainly of coarse-grained sediments such as conglomerate and gritstone with some interbeds of reddish-brown lime-bearing sandstone and siltstone (Figs. 2C and 2D). The upper part is characterized by fine-grained sediments including thick beds of sandstone, siltstone, and mudstone, with some interbeds of conglomerate (Huu et al., 2008). Reddish-brown siltstone beds in the upper part of the formation seldom include thin gypsum veins. The sedimentary facies characteristics indicate deposition in a fluvio-lacustrine environment. The Yen Chau Formation unconformably rests upon many older sedimentary rocks and is covered by Oligocene sedimentary rock. The age of the Yen Chau Formation was formerly assigned to the Late Cretaceous based on its stratigraphic relations and correlation with the evaporite-bearing formations widely distributed in Southeast China, Laos, and Thailand (Khuc, 2000; Thanh and Khuc, 2006). Some freshwater fauna and flora fossils of the Late Cretaceous age, including *Fulpioides* sp., *Helix* sp., and *Angiospermae* were found in the siltstone beds of the Yen Chau Formation (Huu and Luc, 2003). Recently, the detailed magnetostratigraphic ages of evaporite-bearing strata in Southeast Asia have been obtained. For example, the Albian to Paleocene age (>112–63 Ma) is assigned for evaporite-bearing formations in the Simao basin (South China), and the Turonian to Paleocene age (92–63.5 Ma) for the Maha Sarakham Formation in Thailand or the Thangon Formation in Laos (Zhang et al., 2018; Yan et al., 2021). Therefore, the age of the gypsum-bearing Yen Chau Formation is likely from the late Early Cretaceous to the beginning of the Paleocene. The fossils of the brackish-water bivalve *Fulpioides* sp., which occurred in lower Upper Cretaceous strata (Gu et al., 1976), were found in the middle of the lower part of the Yen Chau Formation. This suggests that the base of the Yen Chau Formation was likely deposited during the late Early Cretaceous (Albian?). The boundary between the non-gypsum-bearing middle member and gypsum-bearing upper member of the Mengyejing Formation in the Simao Basin has been dated to approximately 88.7 Ma based on magnetostratigraphic data (Yan et al., 2021). A comparable age (Coniacian) is therefore proposed for the boundary between the lower and upper parts of the Yen Chau Formation, which shows similar lithological characteristics (Fig. 2C). Based on the above information, we propose a mid-Cretaceous age (Albian?–Coniacian?) for the lower part and a Late Cretaceous age (Santonian?–Maastrichtian?) for the upper part of the Yen Chau Formation.

## 3. Materials and methods

A total of 43 fresh mudstone and siltstone samples were collected from the Ban Hang (BH1 – BH16) and Yen Chau Formations (YC1 – YC14 for the lower part and YC15 – YC27 for the upper part) in northern Vietnam. These samples were collected in stratigraphic order and, where possible, at equal stratigraphic intervals.

### 3.1. Geochemical analyses

The geochemical composition of samples was analyzed by X-ray fluorescence (ZSX Primus 2; Rigaku, Tokyo, Japan) at Waseda University, Japan. The samples were milled to <63 μm, dried at 105 °C then heated at 550 °C for 4 h to decompose organic matter before measurement. Fused disks of samples were made with a sample-to-lithium borate ratio of 1:10. Calibration lines were created using reference samples GSJ (JDo-1, JSd-1, JSd-2, JSd-3, JSI-2, JLk-1, JCh-1, JA-2, JA-3, JB-1a, JB-2, JB-3, JG-1a, JG-2, JG-3, JGb-1, JP-1, JR-1, JR-2). The accuracy of calibration lines for all elements was better than 0.6 %. Pressed beads were prepared for trace element abundance measurements with the calibration accuracy better than 8 ppm.

### 3.2. Mineralogical analyses

XRD analyses were performed on oriented samples in air-dried and ethylene glycol-solvated specimens to calculate the clay mineral composition and illite crystallinity (IC). Oriented glass slides of clay minerals (<2 μm fraction separated by sedimentation) were prepared following the standard preparation technique outlined in Moore and Reynolds (1997) including air-dryied (AD), ethylene-glycol solvated (EG) and heated specimens. The specimens were analyzed using a Rigaku X-ray diffractometer (Cu tube, Kα1,2 radiation, 40 kV, 30 mA) at Waseda University, Japan. The clay mineral composition was obtained from the XRD data of oriented samples using the Sybilla software developed by Chevron Inc (Aplin et al., 2006). This software allows for comparing a measured X-ray diffractogram with a modelled pattern of reflection peaks to determine discrete and mixed-layer clay minerals better. The position of basal reflections and their expansion behavior after EG solvation allows the identification of clay minerals and the relative ratio of structural components in mixed-layer phases (Moore and Reynolds, 1997). The abundances of clay minerals were estimated semi-quantitatively based on the intensity and area of (001) reflection on the EG-diffractogram. Illite crystallinity (IC) values, referred to the Kübler Index, were measured as FWHM (full width at half maximum) of the illite d-001 peak (Kübler, 1968; Bozkaya et al., 2011). Additionally, several randomly oriented powder samples with <40 μm size fractions were analyzed by XRD to determine their general mineral composition. The PROFEX software (Doebelin and Kleeberg, 2015) was used for the semi-quantitative determination of essential mineral components.

### 3.3. Geochemical weathering indices

Several chemical weathering indices have been proposed based on different approaches such as unstable mineral decomposition (CIA - Nesbitt and Young, 1982; CIX – Harnois, 1988; PIA – Fedo et al., 1995), labile element mass transfer (WIP; Parker, 1970), and the statistical-empirical technique (W index - Ohta and Arai, 2007). However, these conventional chemical weathering indices should be applied only to the sediments consisting mainly of silicate because the presence of non-silicate materials may lead to

erroneous estimates of weathering intensity. Recently, Cho and Ohta (2022) developed a new weathering index based on statistical–empirical approaches called robust weathering (RW) index to determine the source rock composition and chemical weathering intensity from sediments containing authigenic and biogenic materials. The RW index is calculated from six major element oxides without using $SiO_2$, CaO, and $P_2O_5$ (Cho and Ohta, 2022). In this study, the RW-index (Cho and Ohta, 2022) is used to determine both weathering intensity and source rock type of Cretaceous sediments in northern Vietnam.

## 4. Results

The major and trace element compositions of the Ban Hang and Yen Chau samples are presented in Tables 1 and 2. These data were used to interpret provenance and assess the characteristics of burial diagenesis and paleoweathering processes of these Cretaceous sediments. The whole-rock geochemical composition of Cretaceous sediments in northern Vietnam reveals high concentrations of CaO in some samples of the Ban Hang Formation and in almost all samples from the Yen Chau Formation (Table 1). The XRD investigations on the bulk powders of these samples indicate very high calcite contents (up to 27 %, Fig. 3) suggesting that most of the CaO amount is contributed from non-silicate minerals. Due to the presence of these non-silicate minerals, the conventional weathering indices as CIA, CIX, WIP, and W index are not favoured in paleoweathering assessments, the robust weathering index (RW) is used instead. The RW values calculated for the Ban Hang and Yen Chau samples are presented in Table 1. Generally, RW index shows higher values in the samples in the lower part of the Yen Chau Formation compared to the upper parts and Ban Hang samples.

Clay mineral assemblages from Cretaceous sediments in northern Vietnam are composed of illite, smectite-group mineral, kaolinite, and chlorite (Fig. 4). Illite (10 Å, 5 Å, 3.33 Å peaks) and R3-type illite-smectite mixed-layers with >80 % illite layers (10 Å ~ 11 Å after ethylene-glycol solvation) pooled as illite in general, accounted for more than half of the content in almost all of the clay fraction samples. The smectite phases (~14.5 Å in air-drying conditions, 15 Å ~ 17 Å after ethylene-glycol solvation and 10 Å ~ 12 Å after heating) is identified as dioctahedral vermiculite/smectite mixed layers (diVS-ml) with interstratifications of two

**Table 1**
Major chemical composition and RW values of Ban Hang and Yen Chau samples.

| Formation | Sample | $SiO_2$ | $TiO_2$ | $Al_2O_3$ | $Fe_2O_3$ | MgO | CaO | $Na_2O$ | $K_2O$ | $P_2O_5$ | RW |
|---|---|---|---|---|---|---|---|---|---|---|---|
| Yen Chau (upper unit) | | | | | | | | | | | |
| | YC27 | 63.88 | 0.68 | 12.69 | 4.89 | 0.11 | 2.54 | 11.34 | 0.96 | 2.77 | 40 |
| | YC26 | 67.22 | 0.74 | 13.68 | 5.15 | 0.06 | 2.71 | 6.26 | 1.12 | 2.95 | 39 |
| | YC25 | 67.06 | 0.69 | 12.43 | 4.94 | 0.07 | 2.17 | 8.52 | 1.08 | 2.91 | 39 |
| | YC24 | 59.72 | 0.82 | 15.92 | 6.75 | 0.08 | 3.37 | 8.90 | 0.74 | 3.53 | 50 |
| | YC23 | 65.15 | 0.73 | 10.66 | 4.75 | 0.10 | 1.74 | 13.76 | 0.58 | 2.44 | 50 |
| | YC22 | 61.59 | 0.69 | 10.84 | 4.91 | 0.12 | 3.59 | 14.20 | 1.52 | 2.45 | 29 |
| | YC21 | 60.69 | 0.71 | 12.65 | 5.00 | 0.09 | 2.30 | 15.16 | 0.58 | 2.69 | 51 |
| | YC20 | 59.71 | 0.79 | 16.33 | 6.56 | 0.08 | 2.92 | 9.13 | 0.60 | 3.70 | 54 |
| | YC19 | 68.44 | 0.71 | 10.75 | 4.17 | 0.08 | 1.74 | 10.86 | 1.00 | 2.12 | 39 |
| | YC18 | 67.93 | 0.65 | 10.67 | 4.25 | 0.12 | 2.33 | 10.84 | 1.05 | 2.05 | 36 |
| | YC17 | 57.68 | 0.83 | 16.75 | 7.08 | 0.10 | 3.67 | 9.63 | 0.46 | 3.65 | 59 |
| | YC16 | 64.48 | 0.67 | 11.67 | 4.54 | 0.09 | 2.31 | 12.99 | 0.75 | 2.40 | 44 |
| | YC15 | 63.90 | 0.82 | 13.96 | 5.93 | 0.08 | 3.27 | 8.13 | 0.78 | 2.97 | 46 |
| Yen Chau (lower unit) | | | | | | | | | | | |
| | YC14 | 69.52 | 1.01 | 16.48 | 7.54 | 0.04 | 1.12 | 0.42 | 0.12 | 3.71 | 85 |
| | YC13 | 74.37 | 0.89 | 14.54 | 6.12 | 0.01 | 0.76 | 0.11 | 0.08 | 3.08 | 87 |
| | YC12 | 67.07 | 0.89 | 14.33 | 7.02 | 0.04 | 2.83 | 3.24 | 0.13 | 4.39 | 80 |
| | YC11 | 78.11 | 0.71 | 12.76 | 4.94 | 0.01 | 0.58 | 0.16 | 0.06 | 2.60 | 89 |
| | YC10 | 55.68 | 0.65 | 13.50 | 5.45 | 0.12 | 3.26 | 17.77 | 0.41 | 3.01 | 56 |
| | YC09 | 55.24 | 0.67 | 14.08 | 5.68 | 0.08 | 3.19 | 17.26 | 0.36 | 3.28 | 60 |
| | YC08 | 50.20 | 0.70 | 15.43 | 6.18 | 0.09 | 3.76 | 19.71 | 0.38 | 3.36 | 60 |
| | YC07 | 53.42 | 0.72 | 14.29 | 5.82 | 0.10 | 3.62 | 18.14 | 0.64 | 3.08 | 49 |
| | YC06 | 59.70 | 0.77 | 13.47 | 5.60 | 0.10 | 3.37 | 13.44 | 0.62 | 2.79 | 49 |
| | YC05 | 61.89 | 0.60 | 11.22 | 4.35 | 0.08 | 1.22 | 17.74 | 0.33 | 2.45 | 61 |
| | YC04 | 57.33 | 0.68 | 15.50 | 6.16 | 0.14 | 2.27 | 14.31 | 0.34 | 3.12 | 64 |
| | YC03 | 72.02 | 0.91 | 15.86 | 7.11 | 0.01 | 0.73 | 0.11 | 0.34 | 2.78 | 70 |
| | YC02 | 61.38 | 0.68 | 10.35 | 4.27 | 0.07 | 1.44 | 19.56 | 0.06 | 2.10 | 85 |
| | YC01 | 58.20 | 0.64 | 12.29 | 5.10 | 0.07 | 1.81 | 18.64 | 0.84 | 2.26 | 43 |
| Ban Hang | | | | | | | | | | | |
| | BH16 | 62.89 | 0.73 | 14.02 | 5.72 | 0.07 | 2.46 | 11.15 | 0.44 | 2.38 | 57 |
| | BH15 | 59.59 | 0.75 | 16.66 | 6.55 | 0.07 | 2.55 | 9.90 | 0.46 | 3.32 | 59 |
| | BH14 | 63.43 | 0.93 | 20.73 | 8.13 | 0.02 | 2.51 | 0.15 | 0.54 | 3.49 | 61 |
| | BH13 | 62.34 | 0.88 | 20.23 | 8.46 | 0.08 | 2.73 | 0.72 | 0.44 | 3.94 | 64 |
| | BH12 | 68.58 | 0.84 | 17.78 | 6.84 | 0.01 | 2.08 | 0.10 | 0.47 | 3.24 | 61 |
| | BH11 | 61.98 | 1.07 | 21.40 | 8.75 | 0.02 | 2.68 | 0.10 | 0.41 | 3.54 | 67 |
| | BH10 | 62.13 | 0.89 | 20.24 | 8.55 | 0.18 | 2.03 | 0.52 | 0.58 | 4.68 | 61 |
| | BH09 | 64.91 | 0.90 | 19.50 | 7.88 | 0.16 | 2.07 | 0.13 | 0.41 | 3.95 | 66 |
| | BH08 | 64.18 | 0.91 | 20.23 | 7.57 | 0.13 | 1.96 | 0.13 | 0.48 | 4.29 | 64 |
| | BH07 | 57.37 | 0.72 | 17.01 | 6.59 | 0.06 | 2.36 | 12.00 | 0.46 | 3.27 | 60 |
| | BH06 | 66.04 | 0.84 | 16.11 | 6.96 | 0.04 | 2.02 | 4.72 | 0.53 | 2.65 | 48 |
| | BH05 | 73.05 | 0.91 | 18.03 | 3.14 | 0.01 | 1.08 | 0.53 | 0.80 | 2.43 | 53 |
| | BH04 | 67.41 | 0.91 | 18.75 | 6.96 | 0.05 | 1.45 | 0.45 | 0.57 | 3.40 | 60 |
| | BH03 | 71.24 | 0.94 | 15.62 | 6.64 | 0.05 | 2.53 | 0.10 | 0.34 | 2.49 | 64 |
| | BH02 | 58.38 | 0.70 | 16.72 | 6.19 | 0.09 | 2.77 | 10.34 | 0.62 | 4.04 | 54 |
| | BH01 | 88.25 | 0.58 | 7.36 | 1.45 | 0.09 | 0.62 | 0.11 | 0.36 | 1.15 | 62 |

**Table 2**
Trace element distribution of the Ban Hang and Yen Chau samples.

| Sample | Ba | Co | Cr | Cu | Nd | Ni | Pb | Rb | Sr | Th | V | Y | Zn | Cr | Zr | S |
|---|---|---|---|---|---|---|---|---|---|---|---|---|---|---|---|---|
| Yen Chau (upper unit) | | | | | | | | | | | | | | | | |
| YC27 | 254 | 13 | 106 | 38 | 14 | 52 | 31 | 105 | 106 | 12 | 46 | 30 | 83 | 106 | 192 | 215 |
| YC26 | 253 | 13 | 99 | 43 | 15 | 52 | 21 | 110 | 91 | 14 | 48 | 31 | 90 | 99 | 207 | 86 |
| YC25 | 303 | 13 | 102 | 36 | 13 | 50 | 34 | 110 | 107 | 11 | 82 | 29 | 86 | 102 | 181 | 128 |
| YC24 | 340 | 20 | 96 | 39 | 15 | 54 | 50 | 140 | 100 | 12 | 87 | 32 | 120 | 96 | 156 | 120 |
| YC23 | 190 | 16 | 105 | 36 | 17 | 60 | 36 | 120 | 92 | 11 | 45 | 33 | 106 | 105 | 195 | 132 |
| YC22 | 231 | 15 | 108 | 35 | 17 | 50 | 30 | 92 | 325 | 10 | 46 | 29 | 78 | 108 | 230 | 21,968 |
| YC21 | 212 | 13 | 76 | 35 | 11 | 40 | 37 | 107 | 105 | 10 | 38 | 28 | 80 | 76 | 137 | 163 |
| YC20 | 282 | 24 | 78 | 37 | 13 | 44 | 44 | 130 | 103 | 12 | 65 | 31 | 101 | 78 | 163 | 149 |
| YC19 | 186 | 11 | 87 | 36 | 13 | 37 | 30 | 86 | 93 | 11 | 5 | 29 | 65 | 87 | 260 | 108 |
| YC18 | 169 | 10 | 88 | 35 | 12 | 39 | 24 | 74 | 104 | 8 | 31 | 26 | 54 | 88 | 181 | 172 |
| YC17 | 265 | 19 | 89 | 43 | 13 | 52 | 49 | 135 | 111 | 12 | 55 | 31 | 114 | 89 | 148 | 151 |
| YC16 | 184 | 12 | 83 | 35 | 12 | 39 | 28 | 89 | 100 | 9 | 37 | 27 | 66 | 83 | 173 | 145 |
| YC15 | 217 | 13 | 72 | 32 | 10 | 40 | 33 | 111 | 117 | 9 | 62 | 26 | 68 | 72 | 116 | 115 |
| Yen Chau (lower unit) | | | | | | | | | | | | | | | | |
| YC14 | 259 | 17 | 122 | 32 | 15 | 42 | 57 | 142 | 89 | 12 | 23 | 33 | 94 | 122 | 201 | 57 |
| YC13 | 212 | 15 | 134 | 31 | 15 | 71 | 38 | 143 | 87 | 13 | 77 | 41 | 61 | 134 | 209 | 71 |
| YC12 | 213 | 16 | 146 | 39 | 23 | 76 | 38 | 151 | 98 | 13 | 76 | 40 | 120 | 146 | 314 | 49 |
| YC11 | 280 | 13 | 140 | 47 | 13 | 77 | 87 | 120 | 216 | 10 | 65 | 32 | 31 | 140 | 182 | 60 |
| YC10 | 220 | 13 | 77 | 35 | 10 | 43 | 30 | 100 | 109 | 8 | 56 | 26 | 66 | 77 | 113 | 91 |
| YC09 | 217 | 13 | 72 | 32 | 10 | 40 | 33 | 111 | 117 | 9 | 62 | 26 | 68 | 72 | 116 | 115 |
| YC08 | 260 | 14 | 61 | 34 | 10 | 39 | 39 | 106 | 112 | 9 | 63 | 27 | 70 | 61 | 98 | 130 |
| YC07 | 282 | 13 | 77 | 36 | 10 | 45 | 33 | 104 | 113 | 9 | 62 | 26 | 76 | 77 | 111 | 127 |
| YC06 | 215 | 13 | 70 | 40 | 11 | 43 | 29 | 103 | 91 | 10 | 39 | 27 | 76 | 70 | 124 | 96 |
| YC05 | 201 | 13 | 97 | 36 | 10 | 51 | 40 | 98 | 198 | 8 | 48 | 25 | 64 | 97 | 142 | 145 |
| YC04 | 234 | 15 | 85 | 33 | 10 | 46 | 31 | 101 | 179 | 9 | 84 | 27 | 65 | 85 | 122 | 111 |
| YC03 | 207 | 10 | 106 | 25 | 14 | 40 | 115 | 122 | 704 | 12 | 54 | 32 | 37 | 106 | 258 | 185 |
| YC02 | 140 | 10 | 85 | 25 | 13 | 38 | 31 | 76 | 132 | 9 | 26 | 25 | 48 | 85 | 182 | 87 |
| YC01 | 146 | 12 | 100 | 33 | 9 | 60 | 26 | 73 | 104 | 7 | 143 | 22 | 56 | 100 | 119 | 105 |
| Ban Hang | | | | | | | | | | | | | | | | |
| BH17 | 210 | 14 | 66 | 34 | 11 | 36 | 21 | 99 | 131 | 11 | 74 | 30 | 80 | 66 | 154 | 78 |
| BH16 | 255 | 16 | 95 | 29 | 10 | 46 | 33 | 134 | 140 | 11 | 74 | 31 | 81 | 95 | 133 | 96 |
| BH15 | 392 | 22 | 102 | 40 | 14 | 69 | 34 | 130 | 53 | 13 | 49 | 45 | 128 | 102 | 192 | 40 |
| BH14 | 479 | 21 | 107 | 42 | 13 | 58 | 30 | 165 | 58 | 14 | 115 | 39 | 120 | 107 | 134 | 56 |
| BH13 | 223 | 15 | 116 | 41 | 13 | 61 | 54 | 143 | 61 | 13 | 52 | 36 | 94 | 116 | 144 | 59 |
| BH12 | 459 | 20 | 98 | 36 | 14 | 58 | 49 | 132 | 47 | 14 | 3 | 35 | 130 | 98 | 196 | 65 |
| BH11 | 996 | 19 | 98 | 68 | 14 | 56 | 28 | 179 | 48 | 16 | 61 | 43 | 169 | 98 | 144 | 44 |
| BH10 | 682 | 19 | 91 | 56 | 14 | 53 | 35 | 167 | 57 | 16 | 60 | 37 | 121 | 91 | 154 | 52 |
| BH09 | 729 | 19 | 93 | 53 | 15 | 52 | 21 | 181 | 48 | 17 | 72 | 45 | 138 | 93 | 163 | 54 |
| BH08 | 1001 | 16 | 81 | 23 | 10 | 44 | 31 | 130 | 185 | 11 | 102 | 31 | 87 | 81 | 117 | 231 |
| BH07 | 328 | 14 | 115 | 41 | 14 | 66 | 11 | 192 | 74 | 16 | 74 | 44 | 48 | 115 | 214 | 189 |
| BH06 | 175 | 12 | 115 | 38 | 11 | 53 | 18 | 72 | 42 | 11 | 53 | 26 | 51 | 115 | 254 | 36 |
| BH05 | 68 | 19 | 98 | 23 | 13 | 60 | 31 | 63 | 36 | 15 | 83 | 33 | 33 | 98 | 175 | 58 |
| BH04 | 328 | 16 | 93 | 24 | 12 | 48 | 29 | 166 | 68 | 13 | 55 | 36 | 52 | 93 | 169 | 70 |
| BH03 | 246 | 14 | 119 | 26 | 15 | 37 | 26 | 118 | 35 | 16 | 27 | 42 | 54 | 119 | 239 | 72 |
| BH02 | 549 | 17 | 79 | 31 | 11 | 41 | 29 | 144 | 125 | 12 | 85 | 42 | 94 | 79 | 124 | 167 |
| BH01 | 836 | 65 | 94 | 77 | 13 | 133 | 38 | 167 | 67 | 13 | 78 | 84 | 344 | 94 | 145 | 80 |

smectite members having d-spacing of ~13 Å and ~17 Å in ethylene glycol-saturated state (SS di-GLY in Sybilla fitting; Fig. 4C). The proportion of non-expandable smectite members (dioctahedral vermiculite) in diVS-ml varied from 50 % to 90 % in the analyzed samples. The diVS-ml constituted 20 % on average of the clay minerals in the Ban Hang and Yen Chau samples and referred to as smectite for the interpretation of paleoweathering intensity and paleoclimate variation. Kaolinite (7.18 Å and 3.58 Å peaks that disappeared on heated specimen) and chlorite (14.2 Å, 7.1 Å, 4.74 Å and 3.56 Å peaks) occurred jointly in all samples with varied proportions. Although there is a similarity of d-spacing of kaolinite and chlorite at ~7 Å and ~3.5 Å, the presence of chlorite is confirmed by the existence of its reflections (but much weakened) after heat treatment at 550 °C for 2 h (Moore and Reynolds, 1997). The clay mineral compositions of Ban Hang and Yen Chau samples are summarized in Table 3 and visualized in Figs. 5 and 6. The general character of the clay assemblages demonstrates the lower levels of kaolinite and smectite compared to illite in all samples but kaolinite content increases in the lower part of the Yen Chau Formation. The samples from Ban Hang Formation have higher proportions of chlorite.

## 5. Discussion

### 5.1. Provenance stability

The source-rock composition is the primary factor controlling the bulk geochemical and clay-mineral composition of sedimentary rocks (e.g., Taylor and McLennan, 1985; McLennan et al., 1993). Accordingly, if stratigraphic variations in source rock are present, these would affect the geochemical signatures related to paleoclimate change. Therefore, provenance analysis should be conducted before reconstructing the paleoclimate. This study estimates the source-rock composition based on ratios of incompatible to compatible trace elements, ternary diagrams of geochemistry and clay mineral composition. Ratios of compatible to incompatible trace elements are widely used for monitoring the source-rock composition (e.g., McLennan, 1993; Ohta et al., 2011;

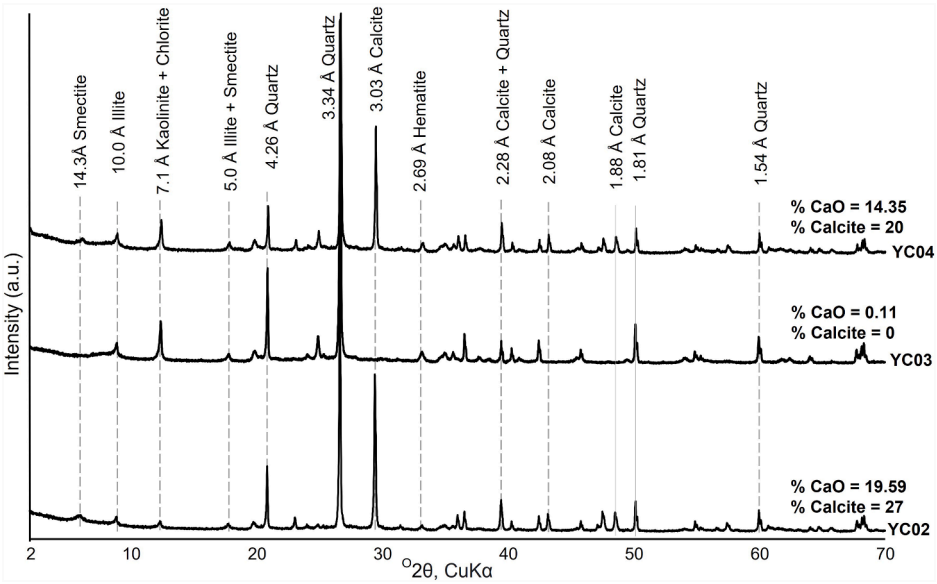


**Fig. 3.** Representative XRD patterns (bulk samples) of Yen Chau mudstones. Semi-quantitative determination of mineral components using PROFEX software indicates CaO concentrations in Yen Chau samples are mainly contributed by calcite.

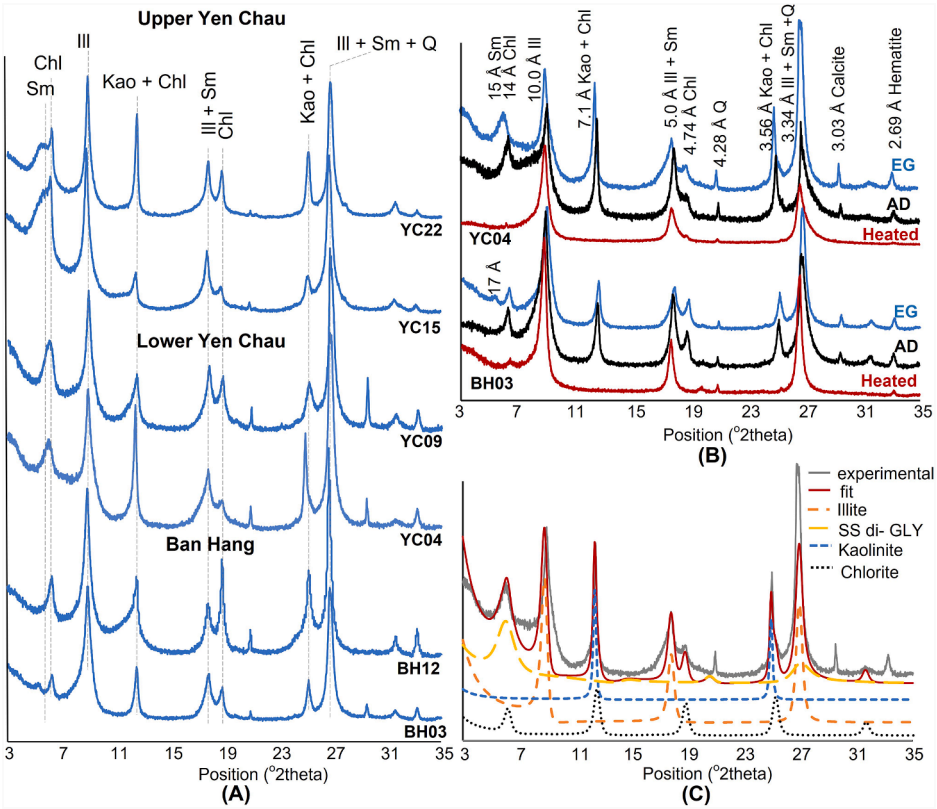


**Fig. 4.** X-ray diffractograms of oriented specimens: (A) XRD patterns of representative samples of Ban Hang and Yen Chau Formations. (B) Comparison of XRD patterns between air-dried (AD), ethylene glycol-solvated (EG), and heated specimens. Notes: Sm = Smectite; Ill = Illite; Kao = Kaolinite; Chl = Chlorite; Q = Quarzt. (C) Sybilla software modelling from XRD patterns of oriented specimens. Notes: experimental = XRD data; fit = refined XRD data; SS di-GLY = dioctahedral smectite–smectite interstratifications in ethylene-glycol-saturated state.

Luo et al., 2015; Dinis et al., 2016), because such ratios clearly distinguish mafic from felsic igneous source rock, thereby facilitating provenance analysis. Figure 5A shows Y/Ni–Co/Th diagrams, in which sediments sourced from felsic rock are plotted in the upper left region, and those from mafic rocks in the lower right. The Y/Ni and Co/Th values of the Ban Hang and Yen Chau Formations are 0.3–1.1 and 0.8–2.0, respectively, showing a similar composition to that of andesite to granodiorite (Fig. 5A). The 95 %

**Table 3**
Clay minerals composition of Ban Hang and Yen Chau samples.

| Formation | Sample | Illite | Kaolinite | Chlorite | diVS-ml | %V |
|---|---|---|---|---|---|---|
| Yen Chau (upper unit) | | | | | | |
| | YC27 | 63 % | 6 % | 10 % | 21 % | 57 |
| | YC26 | 57 % | 3 % | 15 % | 25 % | 54 |
| | YC25 | 53 % | 5 % | 11 % | 31 % | 54 |
| | YC24 | 54 % | 8 % | 14 % | 24 % | 56 |
| | YC23 | 62 % | 12 % | 4 % | 22 % | 53 |
| | YC22 | 50 % | 10 % | 32 % | 8 % | 51 |
| | YC21 | 79 % | 4 % | 2 % | 15 % | 51 |
| | YC20 | 56 % | 5 % | 1 % | 38 % | 53 |
| | YC19 | 75 % | 15 % | 1 % | 9 % | 54 |
| | YC18 | 53 % | 3 % | 6 % | 38 % | 54 |
| | YC17 | 58 % | 5 % | 15 % | 22 % | 65 |
| | YC16 | 55 % | 9 % | 11 % | 25 % | 57 |
| | YC15 | 51 % | 11 % | 10 % | 28 % | 61 |
| Yen Chau (lower unit) | | | | | | |
| | YC14 | 88 % | 9 % | 3 % | N.A. | N.A. |
| | YC13 | 70 % | 29 % | 1 % | N.A. | N.A. |
| | YC12 | 74 % | 5 % | 3 % | 18 % | 53 |
| | YC11 | 68 % | 30 % | 2 % | N.A. | N.A. |
| | YC10 | 57 % | 14 % | 8 % | 21 % | 59 |
| | YC09 | 51 % | 15 % | 5 % | 29 % | 57 |
| | YC08 | 42 % | 9 % | 9 % | 40 % | 57 |
| | YC07 | 52 % | 11 % | 10 % | 27 % | 59 |
| | YC06 | 50 % | 17 % | 8 % | 25 % | 59 |
| | YC05 | 51 % | 33 % | 16 % | N.A. | N.A. |
| | YC04 | 45 % | 26 % | 9 % | 20 % | 67 |
| | YC03 | 67 % | 30 % | 3 % | N.A. | N.A. |
| | YC02 | 60 % | 30 % | 1 % | 9 % | 50 |
| | YC01 | 47 % | 21 % | 11 % | 21 % | 61 |
| Ban Hang | | | | | | |
| | BH16 | 57 % | 3 % | 27 % | 13 % | 58 |
| | BH15 | 63 % | 5 % | 15 % | 17 % | 65 |
| | BH14 | 52 % | 11 % | 18 % | 19 % | 66 |
| | BH13 | 61 % | 2 % | 11 % | 26 % | 83 |
| | BH12 | 51 % | 3 % | 30 % | 16 % | 70 |
| | BH11 | 61 % | 10 % | 11 % | 18 % | 61 |
| | BH10 | 55 % | N.A. | 16 % | 29 % | 52 |
| | BH09 | 59 % | 1 % | 14 % | 26 % | 86 |
| | BH08 | 58 % | 14 % | 10 % | 18 % | 64 |
| | BH07 | 79 % | 5 % | 6 % | 10 % | 60 |
| | BH06 | 67 % | 8 % | 2 % | 23 % | 83 |
| | BH05 | 46 % | 8 % | 11 % | 35 % | 79 |
| | BH04 | 51 % | 14 % | 16 % | 19 % | 69 |
| | BH03 | 51 % | 6 % | 27 % | 16 % | 74 |
| | BH02 | 51 % | N.A. | 36 % | 13 % | 77 |
| | BH01 | 58 % | 5 % | 10 % | 27 % | 72 |

diVS-ml = dioctahedral vermiculite/smectite mixed layers, %V = proportion of vermiculite in diVS-ml.

confidence regions of the population mean values for the Ban Hang and Yen Chau Formations show a clear overlap. This result suggests that these formations have identical provenance, and the bulk geochemical composition of the source rocks is comparable to that of intermediate igneous rocks (between granodiorite and andesite).

The mafic-felsic-RW diagram (Cho and Ohta, 2022) allows illustrating the weathering trend of sedimentary rock and the source rock composition can be estimated simply by tracing the weathering trend back to the unweathered domain. Particularly, the compositional variation of igneous rocks is represented by mafic to felsic apices and each weathering profile is plotted as a trend from unweathered source rock toward the RW apex. Figure 5B illustrates the hinterland weathering trend of the Ban Hang and Yen Chau formations, represented by a single regression line (94.78 % of variance explained), which extends backward to the unweathered domain of intermediate igneous rock composition. This means both formations were sourced from intermediate igneous rock with similar compositions. The ternary diagram of clay mineral composition (Fig. 5C) also indicates consistent results.

The Cr/Zr ratio is also used as another provenance index to evaluate the contribution of mafic and felsic rocks in a sediment source, as the concentrations of these two elements reflect the distribution of ultramafic and granite components (Wronkiewicz and Condie, 1987). Cr is mainly derived from mafic rocks while Zr is specifically abundant in felsic rocks. The similarity of the Cr/Zr ratio between the Ban Hang and Yen Chau samples (average 0.59) suggests an identical source for the Cretaceous sediments (Fig. 6D). Similarly, the $Al_2O_3/TiO_2$ ratio varies considerably for the pristine igneous source rock but remains constant in most weathering regimes, thus it is considered as a reliable indicator of provenance (Young and Nesbitt, 1998). Figure 6E reveals an insignificant fluctuation in the $Al_2O_3/TiO_2$ ratio between the Ban Hang and Yen Chau sediments, indicating negligible changes in provenance. The fact that nearly all samples fall between 8 and 21 indicates the intermediate igneous provenance of these formations (Roser and Korsch, 1988; Cai et al., 2022). The slightly elevated $Al_2O_3/TiO_2$ ratio (above 21) in some Ban Hang samples is likely due to a minor increase in felsic compositions. This has an insignificant impact on the interpretation of paleoclimate.

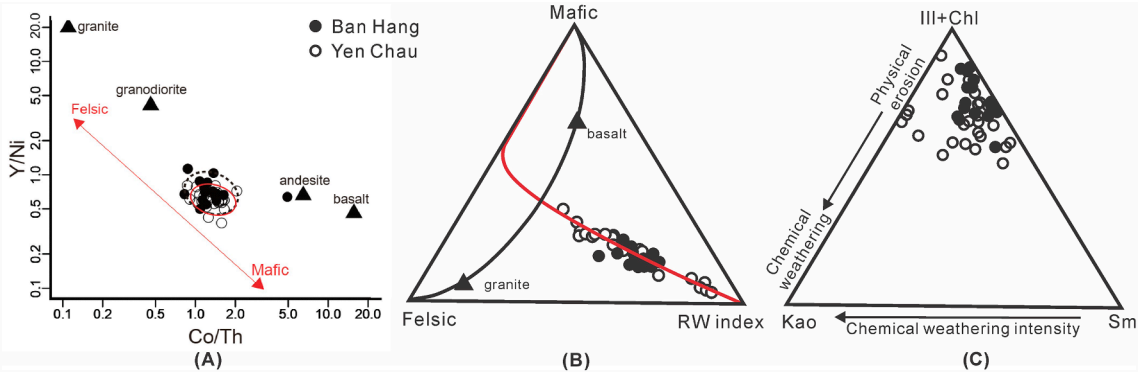


**Fig. 5.** Reconstruction of source rock composition of Ban Hang and Yen Chau Formations. (A) Plots of Co/Th–Y/Ni diagram. Black dotted ellipse represents 95 % confidence region of population mean values for Ban Hang Formation and red solid ellipse for that of Yen Chau Formation. Also shown for comparison are typical granite, granodiorite andesite and basalt compositions. (B) The Mafic-Felsic-RW ternary diagram (after Cho and Ohta, 2022). Red line shows the regression line of studied samples. Black line represents the compositional linear trend for fresh igneous rocks. (C) Ternary diagram of clay mineral assemblages. Provenance sources and alteration processes are also indicated (after Hu et al., 2014).

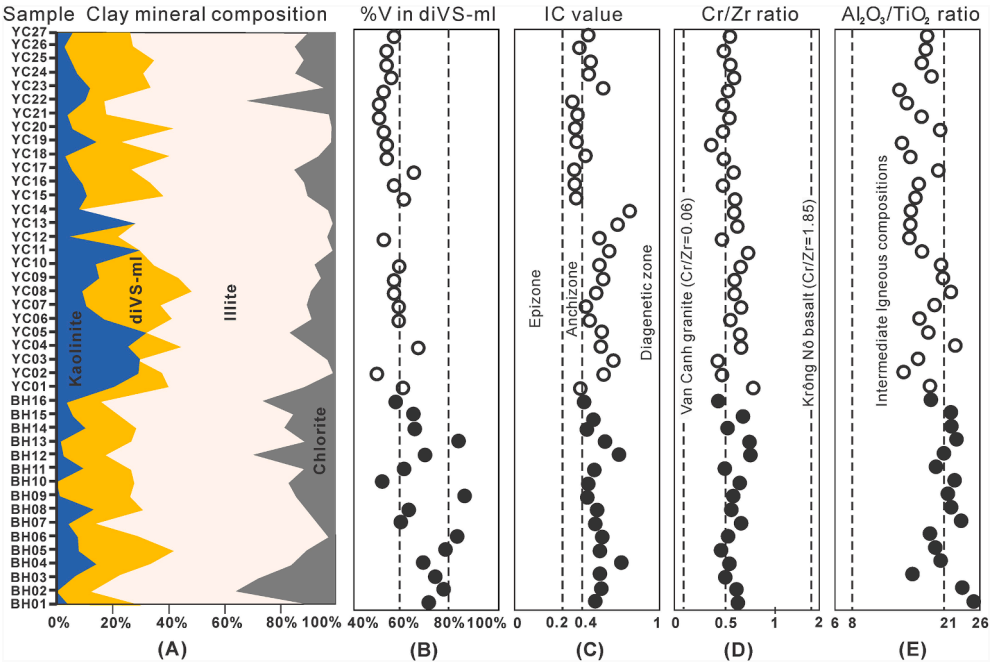


**Fig. 6.** Distribution of diagenesis and provenance indicators in Ban Hang and Yen Chau sediments: (A) Clay minerals composition; (B) Proportion of vermiculite component in dioctahedral vermiculite/smectite mixed layers (diVS-ml); (C) Value of illite crystallinity - (IC). Low-grade metamorphic zones are indicated according to Blenkinsop (1988). (D) Cr/Zr ratios. Dashed lines indicate average Cr/Zr values of typical Vietnamese granite and basalt (data from Hung et al., 2022; Hoang et al., 2019). (E) $Al_2O_3/TiO_2$ ratios. $Al_2O_3/TiO_2$ values from 8 to 22 indicate intermediate igneous provenance (Cai et al., 2022).

### 5.2. Diagenesis evaluation

In addition to the initial content of source rocks, burial diagenesis may alter the chemical and mineralogical compositions of sedimentary rock, therefore its influence should be evaluated before discussing the hinterland weathering and paleoclimate. The transformation from smectite to illite is a common diagenesis process in sedimentary rock. During this process, multi-member mixed-layer clay minerals including dioctahedral vermiculite/smectite mixed layers (diVS-ml) and illite/smectite mixed layers (IS-ml) are formed as intermediate products of reactions (Curtis, 1985; Velde and Vasseur, 1992; Meunier et al., 2000, 2004). During the illitization process, the formation of dioctahedral vermiculite layers from montmorillonite is transitional stage in prior to the precipitation of illite layers of fixed chemical composition (Meunier et al., 2000; Lanson et al., 2009; Cifuentes et al., 2021). Therefore, the presence of diVS-ml indicates that the illitization of smectite was only in the early stages. It means that the sedimentary rocks of the Yen Chau and Ban Hang Formations belong to the low-moderate diagenesis stage. The proportion of vermiculite layers in diVS-ml increased from the younger Yen Chau formation ($\%V = 50–60$ %) to the older Ban Hang formation ($\%V = 60–90$ %), thus, this trend depicted in Fig. 6 is concordant with stratigraphical positions of strata.

The diagenetic effects were also evaluated by means of the illite crystallinity (IC) values in that degree of diagenesis into the diagenetic zone (IC > 0.4), the anchizone (IC = 0.215–0.4), and the epizone (IC < 0.215) with intensification of metamorphism (Blenkinsop, 1988). Almost all IC values obtained from the studied samples belong the diagenetic zone, indicating a minor effect of diagenesis. Several samples in the upper part of the Yen Chau Formation have slightly lower IC values and are classified into anchizone. However, it is unrealistic to assume that only upper horizons underwent deep burial and high-grade diagenesis. These higher-grade illites are probably detrital in origin, derived from a metamorphic terrane. Therefore, it can be concluded that the diagenetic effect is negligible and the geochemical and clay mineralogical characteristics during deposition seem to have remained unaltered.

### 5.3. Paleoweathering intensity and paleoclimate variation across the Cretaceous in northern Vietnam

The mineralogy and geochemistry of mudstones are controlled mainly by hinterland paleoweathering, source-rock composition, and diagenesis. However, as discussed above, the source-rock composition and diagenetic effects were identical for the Ban Hang and Yen Chau Formations. Therefore, the mineralogical and geochemical differences between these formations are attributed to differences in the degree of paleoweathering and/or paleoclimate conditions. In this study, the paleoweathering and paleoclimate variation of northern Vietnam in the Cretaceous will be attested to by utilizing clay-mineral composition and geochemical weathering indices.

Past weathering intensity is vital to understand paleoclimate conditions, so it is mentioned in almost all paleoclimate studies. In particular, chemical weathering of silicates is a crucial process considered the most important mechanism for regulating long-term climate change and stabilizing Earth's climate system (e.g., Walker et al., 1981; Berner et al., 1983; Penman et al., 2020). As mentioned in Section 3.3, the robust weathering index (RW) is used to determine the weathering intensity and climate conditions of these Cretaceous sediments, rather than conventional indices, due to the abundance of non-silicate minerals. Cho and Ohta (2022) integrated the RW values of recent soils developed in tropical rainforest to arctic climates and the RW values obtained in this study are compared with them to assess the paleoclimate of northern Vietnam in the Cretaceous (Fig.7). The RW values of mudstones from the Ban Hang Formation and the upper part of the Yen Chau Formation were plotted between 40 and 65, which are

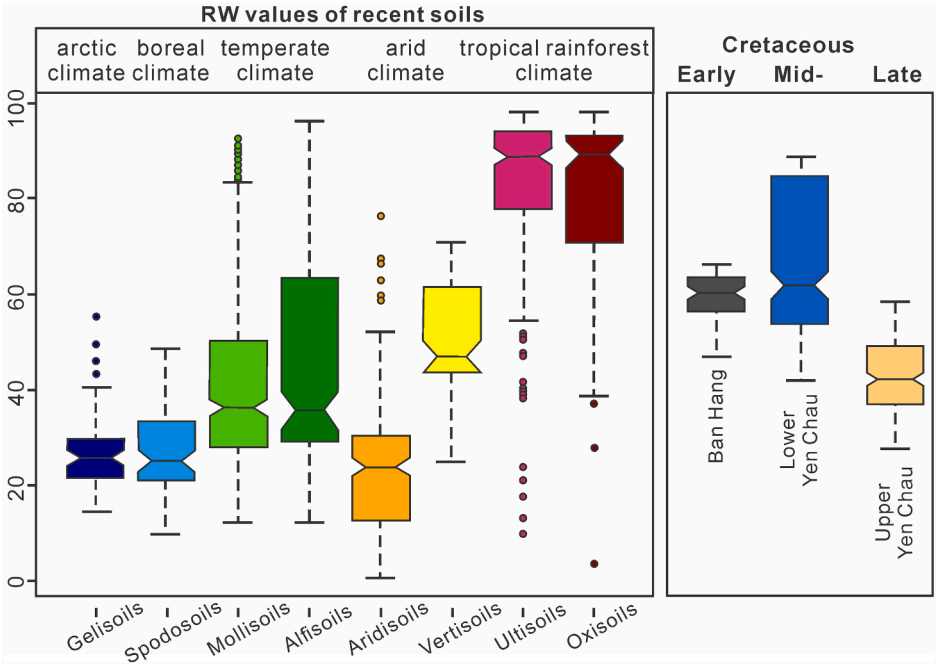


**Fig. 7.** Comparison of the RW values of recent soils developed under different climate zones (Cho and Ohta, 2022) and those of the northern Vietnam mudstones.

equivalent to those of soils developed in arid or temperate climates. The RW values of samples from the upper part of the Yen Chau Formation were smaller than those of the Ban Hang samples, indicating a weaker intensity of paleoweathering in the Late Cretaceous in comparison with the Early Cretaceous. The RW values of the samples from the lower part of the Yen Chau Formation were distributed mainly in the range of 50–85, indicating that northern Vietnam experienced a higher degree of paleoweathering in the mid-Cretaceous. The RW values more likely suggest a warmer and wetter climate in the mid-Cretaceous, comparable to temperate and tropical rainforest climates, based on the RW values.

Clay minerals are the weathered products of rock-forming silicate minerals and are thus widely used for reconstructing the paleoweathering process and paleoclimate conditions (Robert and Chamely, 1991; Baioumy, 2004; Xu et al., 2017; Ye et al., 2022). Kaolinite is commonly formed under warm and humid climates with effective leaching conditions whereas illite and chlorite are primary clay minerals derived from the physical erosion of bedrock under relatively dry conditions (Millot, 1970; Chamley, 1989; Liu et al., 2004). The formation of smectite also requires a warm climate but one less humid than that needed for kaolinite formation (Chamley, 1989; Velde, 1995; Liu et al., 2007). The ratios of specific clay minerals, which form under distinct conditions, are reliable indicators for assessing the paleoweathering and paleoclimate conditions of different geological periods (Thamban et al., 2002; Limmer et al., 2012; Das et al., 2013; Hu et al., 2014; Alizai et al., 2014; Hadji et al., 2019). In this study, we refer to chemical weathering indices including kaolinite/(illite + chlorite) and (smectite + kaolinite)/(illite + chlorite) ratios and humidity index, that is, the ratio of kaolinite to illite.

Generally, the Ban Hang and Yen Chau samples exhibit clay mineral composition characterized by high illite and low kaolinite contents (Fig. 6A). This suggests that physical erosion was predominant, and humidity was low in northern Vietnam during the Cretaceous. The ternary diagram of clay mineral assemblages (Fig. 5C) also shows a significant increase in chemical weathering in the lower part of the Yen Chau Formation, although physical erosion still prevailed. Thus, the weathering conditions were not stable throughout the studied section but showed apparent variation. Figure 8 shows the variation in climate conditions throughout the Cretaceous. The high quantity of kaolinite in the lower part of the Yen Chau Formation indicates a warmer and wetter climate during the mid-Cretaceous compared with the Early and late Cretaceous intervals. Conversely, the Early Cretaceous is believed to be the coldest interval, characterized by the highest levels of chlorite and illite. In addition to the geochemical weathering indicator (RW index), the higher value of kaolinite/(illite + chlorite) and (smectite + kaolinite)/(illite + chlorite) ratios in the lower part of the Yen Chau Formation also demonstrate a significant increase in chemical weathering intensity in the mid-Cretaceous. The higher value of humidity proxies including kaolinite content and kaolinite/illite ratio reflect slight humidification of northern Vietnam during the mid-Cretaceous.

The intensity of chemical weathering can be promoted by an increase in temperature and/or humidity. The increase in temperature during the mid-Cretaceous is not controversial, as this interval is known to be the warmest and to have had the highest atmospheric $CO_2$ concentration during the Cretaceous (Wang et al., 2014; Tabor et al., 2016; Forster et al., 2017). Previous studies have reported extremely high temperatures (exceeding 40 °C in the Khorat plateau, Thailand) during the Cenomanian–Santonian interval, in contrast to the much lower temperatures (<25 °C) recorded during the Early and Late Cretaceous (Amiot et al., 2015; Li et al., 2020). The high level of global temperature and $CO_2$ concentration contributed significantly to the enhancement of the hinterland paleoweathering rate. The geochemical weathering indices from the mudstone of the Sichuan basin also indicated an intensification of hinterland paleoweathering during the mid-Cretaceous. This was induced by a global temperature rise (Cho et al., 2019), although semi-arid to arid climates generally prevailed (Li et al., 2016; Li J. et al., 2018). However, in addition to chemical weathering proxies, this study recorded a significant increase in kaolinite content from the Ban

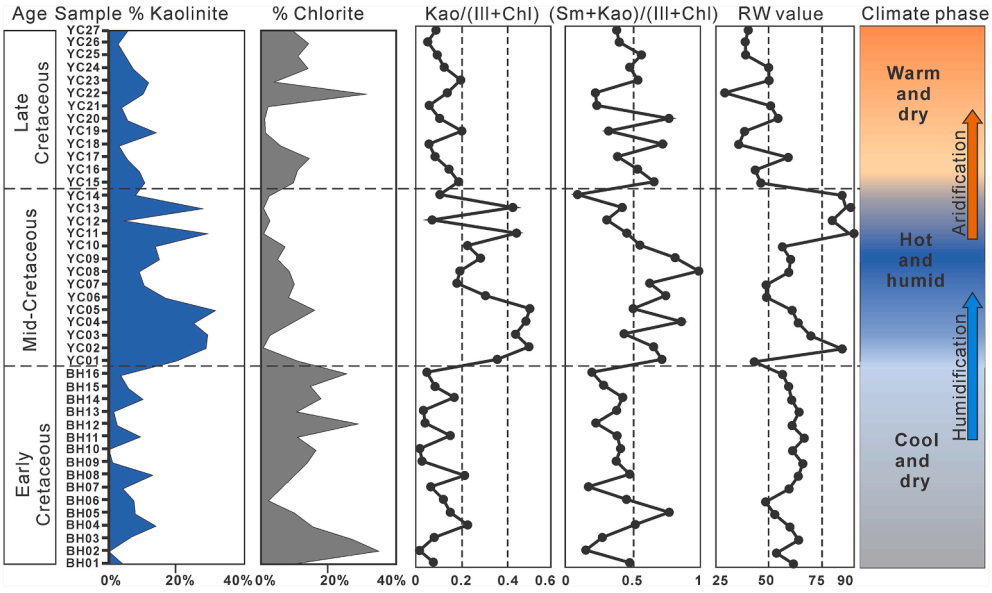


**Fig. 8.** Variations in climate-sensitive proxies from sediment samples show the climate change in northern Vietnam across the Cretaceous Period. Note: Kao/(Ill + Chl) = kaolinite/(illite + chlorite) ratio; (Sm + Kao)/(Ill + Chl) = (smectite + kaolinite)/(illite + chlorite) ratio.

Hang Formation (average 9 %) to the lower part of the Yen Chau Formation (average 20 %). Since kaolinite typically results from highly hydrolytic weathering reactions, we propose that an increase in humidity, coupled with a rise in temperature, occurred from the Early to mid-Cretaceous.

Conclusively, all geochemical weathering and clay-mineralogy indicators agreed to indicate the climate variation that occurred in northern Vietnam throughout the Cretaceous. Specifically, northern Vietnam is proven to have experienced a cool and temperate climate in the Early Cretaceous and to have shifted to a hot and sub-humid climate in the mid-Cretaceous then became warm and arid in the Late Cretaceous. Thus, the study results indicate two climate change trends that occurred in the Cretaceous, including slight humidification from the Early to mid-Cretaceous, accompanied by an increase in chemical weathering intensity and aridification from the mid-to Late Cretaceous.

### *5.4. Climate differentiation between the margin and interior of Southeast Asian continent during the Cretaceous*

The Cretaceous paleoclimate of the Southeast Asian continent has been the subject of numerous studies. These investigations have relied on climate-sensitive sediments and fossils from sedimentary basins, including those in Sichuan, Simao, and Khorat (Jiang and Li, 1996; Hasegawa et al., 2010, 2012; Wu et al., 2017; Li G. et al., 2018; Wang et al., 2021; Wang et al., 2022). Investigated Cretaceous basins are primarily located within the continental interior, where climatic conditions are greatly influenced by regional geological factors. Investigating the paleoclimate of coastal regions, such as Vietnam, is anticipated to yield actual climate information of Southeast Asia area.

The results of this study reveal a contrasting climate condition in the Cretaceous between the Southeast Asian continental margin (Vietnam) and the inland areas of Southeast Asia. During the Early Cretaceous, a temperate and semi-arid climate with intermittent sub-humid episodes was prevalent in South China (Sichuan Basin) and Thailand (Khorat Basin) (Horiuchi et al., 2012; Amiot et al., 2015; Li et al., 2016), whereas the Simao Basin was characterized by a warm and humid climatic regime, as indicated by the predominance of fluvio-lacustrine sediments (Wu et al., 2004; Wu et al., 2017). As for this interval (Early Cretaceous), this study revealed that Vietnam experienced a temperate climate similar to that of South China and Thailand. In contrast, previous studies have revealed an extremely arid climate in Southeast Asian inland areas during the mid-Cretaceous and Late Cretaceous by the presence of aeolian and evaporite deposits in all Sichuan, Simao, and Khorat basins (Jiang and Li, 1996; Hasegawa et al., 2010, 2012; Wu et al., 2017; Li G. et al., 2018). However, the climate in Vietnam during the mid-Cretaceous was likely warmer and wetter than in the early and late stages, leading to a significant increase in chemical weathering. The slight increase in humidity in Vietnam from the Early to mid-Cretaceous indicates a different climate change trend in marginal areas compared to the interior of the Southeast Asian continent. In the Late Cretaceous, a predominantly arid climate prevailed in broader areas of the Southeast Asian continent. This indicates aridification in the low latitudes of the Northern Hemisphere, although the marginal areas were not as dry as the inland regions. These comparisons highlight the climate differences between the continental interior and marginal regions, which were particularly pronounced during the mid-Cretaceous.

Previous studies indicate that the Cretaceous climate in Southeast Asia was configured by both planetary circulations and paleo-geographic configuration. The palaeogeographical reconstruction of Southeast Asia during the Cretaceous intervals is presented in Fig. 9. The Simao, Sichuan, and Khorat basins were situated further north and more inland than their current locations (Yang and Besse, 1993; Sato et al., 1999). Moreover, the highlands created by the collision of Sibumasu with Indochina/East Malaysia were already present on the west side of the Southeast Asian continent during the Cretaceous. These highlands might have protected the interior basins from ocean moisture (Metcalfe, 2011; Metcalfe, 2013). During the Early Cretaceous, Southeast Asia maintained a semi-arid climate that alternated with semi-humid phases, due to the prevalence of monsoonal circulation (Jiang and Li, 1996; Jiang et al., 2001). The Simao Basin was situated near the eastern margin of the weakening megamonsoon region and was therefore influenced by both warm, humid air masses and

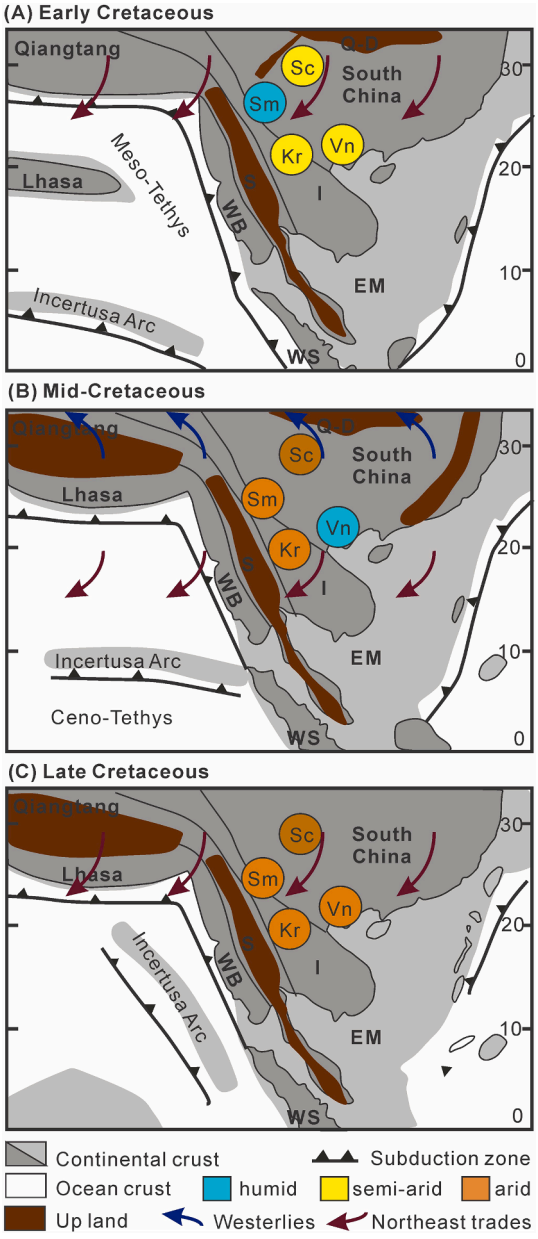


**Fig. 9.** Palaeogeographical reconstructions for Southeast Asia in (A) Early Cretaceous, (B) Mid-Cretaceous, and (C) Late Cretaceous (modified after Metcalfe, 2013; Zhang et al., 2016; Tian et al., 2021). The climatic characteristics of the basins are derived from previous studies, including Jiang and Li (1996), Wu et al. (2004, 2017) for the Simao Basin; Li et al. (2016), Li J. et al. (2018), and Li G. et al. (2018) for the Sichuan Basin; and Horiuchi et al. (2012) and Wang et al. (2021) for the Khorat Basin. S = Sibumasu; WB = West Burma, WS = West Sumatra, EM = East Malaya, I = Indochina, Sc = Sichuan Basin, Sm = Simao Basin, Kr = Khorat Basin, Vn = Northern Vietnam.

the arid subtropical high-pressure system (Fang et al., 2016). Furthermore, Zhang et al. (2025) proposed that, despite the closure of the Meso-Tethys Ocean in the eastern Qiangtang Terrane, a residual sea may have persisted adjacent to the Simao Basin during the earliest Cretaceous (before 142.3 Ma). The potential influence of regional tectonic activities during later stages on the prevailing climatic conditions is also not ruled out. These combined factors likely contributed to the relatively more humid conditions observed in the Simao Basin compared to neighboring basins.

In the mid-Cretaceous, the subtropical high-pressure belt is believed to have shifted from mid-latitude to low-latitude position. This shift was attributed to the equatorward shrinkage of the Hadley circulation, leading to an arid climate zone on the Southeast Asian continent (Hasegawa et al., 2012). Furthermore, the closure of the Mesotethys Ocean and continuous orogeny from topographic uplift in East Asia throughout the Cretaceous Period (especially the mid-Cretaceous) resulted in mountain systems. These barriers blocked moisture transport from both the Tethys and Pacific oceans to the inland, thereby intensifying the aridification of the inland. Specifically, the collision of the Lhasa Block and the Qiangtang Block led to the formation of uplifted areas along the Bangong-Nujiang suture zone (Metcalfe, 2013; Zhu et al., 2022). This caused the interior basins to become more enclosed. During this interval, the accretion of West Burma and other small terranes to Southeast Asia resulted in significant topographical uplift in Southeast China and Indochina. This uplift included the Jiangnan Domain, the Ailaoshan Suture, and the Gaoligong-Baoshan mountain range. The orographic rain shadow effect, caused by these uplift structures, intensified the process of desertification in inland areas (Yu et al., 2014; Li et al., 2016; Wu et al., 2017; Li G. et al., 2018). Specifically, the coastal mountain range on the eastern margin of South China formed due to the Okhotomorsk-East Asia collision during the mid-Cretaceous (100–85 Ma) (Yang, 2013; Zhang et al., 2016). This coastal mountain range not only obstructed the transport of water vapor from the ocean to the continent but also produced a “pumping” effect. This effect drew moisture from both the ocean and interior Asia, causing precipitation over the mountain and the surrounding region (Zhang et al., 2021a). This is considered as a primary factor causing climate differences between the interior and continental margin of Southeast Asia. Thus, northern Vietnam, being the outermost southern coastal margin of the South China block, was generally wetter than inland areas due to its easy supply of ocean moisture. Other regions along the South China coastline, including eastern Jiangxi, Zhejiang, and Guangdong, also indicate a warm and humid climate during the mid-Cretaceous (Li et al., 2009; Wang et al., 2022). The atmosphere-ocean general circulation models used in the studies by Zhang et al. (2021a) demonstrated a significant intensification of precipitation with the increase in mountain height and global $CO_2$ concentration. This explains the significant difference between the continental margin and inland climate during the mid-Cretaceous when the mountain height was at its peak and $CO_2$ concentration increased dramatically. During the Late Cretaceous, the altitude of mountain ranges decreased significantly due to intensive weathering, and combined with a global temperature decline, which led to the maintenance of an arid climate.

This study presents evidence that supports climate differentiation between coastal areas and inland basins. This is further evidenced by the distribution and characteristics of evaporite deposits. That is, thick layers of halite and anhydrite are found throughout evaporite-bearing formations in the Khorat Plateau (Tabakh et al., 1999; Zhang et al., 2018; Li et al., 2020). In contrast, the upper part of the Yen Chau formation has thin gypsum veins (2–3 cm: Sakai et al., 2006; Huu et al., 2008). During evaporation, calcium carbonate and gypsum start to precipitate at a significantly lower brine concentration than halite and anhydrite (McCaffrey et al., 1987; Herrero et al., 2015). Therefore, the widespread presence of halite and anhydrite in Khorat deposits suggests a high degree of evaporation in an extremely arid environment. Therefore, it can be concluded that inland basins

underwent more intense and prolonged aridification compared to coastal areas due to the impact of regional tectonic configuration.

## 6. Conclusion

Geochemical and clay mineral compositions of mudstone samples recovered from northern Vietnam were investigated to assess the hinterland paleoweathering and paleoclimate conditions in the Cretaceous. The mineralogy and geochemistry characteristics of Cretaceous sediments were suggested to be affected insignificantly by burial diagenesis and provenance but indicated the variation in paleoweathering and paleoclimate conditions throughout the Cretaceous Period. Northern Vietnam's climate was proven to shift from a cool and temperate climate in the Early Cretaceous to a hot and sub-humid climate with the clear enhancement of chemical weathering intensity in the mid-Cretaceous. Then it remained under arid conditions to the Late Cretaceous. The climate conditions of northern Vietnam were generally not as arid as those of Thailand and South China's inland regions, indicating climate discrimination between the coastal and interior parts of the Southeast Asian continent. The slight humidification along the Southeast Asian continent margin during the mid-Cretaceous resulted from the "pumping" effect of the coastal mountain range and the increase in water vapor due to global warming, whereas the rain-shadow effect from regional orogenic activities intensified inland aridification. These results suggest that the continent's climate characteristics are significantly influenced by global atmospheric circulation and regional geographical and tectonic factors.

## CRediT authorship contribution statement

**Pham Thi Nga:** Writing – original draft, Visualization, Investigation. **Taro Higuchi:** Writing – original draft, Investigation. **Kentaro Oe:** Investigation. **Nguyen Quoc Dinh:** Investigation. **Rajat Mazumder:** Investigation. **Tohru Ohta:** Writing – review & editing, Supervision.

## Declaration of competing interest

The authors declare the following financial interests/personal relationships which may be considered as potential competing interests: Tohru Ohta reports financial support was provided by Japan Society for Promotion of Science. Tohru Ohta reports financial support was provided by Waseda University Grant for Special Research Project. If there are other authors, they declare that they have no known competing financial interests or personal relationships that could have appeared to influence the work reported in this paper.

## Acknowledgments

We are deeply grateful to the anonymous reviewers for their insightful comments and valuable suggestions, which significantly enhanced the quality of this manuscript. We also sincerely thank the Editor-in-Chief, Prof. Maria Rose Petrizzo, and the Associate Editor, Dr. Mathieu Martinez, for their careful and thoughtful handling of our paper. This work was financially supported by the Waseda University Grant for Special Research Project A (2017A-16; T. Ohta) and the Japan Society for the Promotion of Science (18K03787; T. Ohta).

## Data availability

Data will be made available on request.

## References

Alizai, A., Hillier, S., Clift, P.D., Giosan, L., Hurst, A., VanLaningham, S., Macklin, M., 2014. Clay mineral variations in Holocene terrestrial sediments from the Indus Basin. Quaternary Research 77, 368–381.

Amiot, R., Wang, X., Zhou, Z., Wang, X., Lecuyer, C., Buffertaut, E., Fluteau, F., Ding, Z., Kusuhashi, N., Mo, J., Phillippe, M., Suteethorn, V., Wang, Y., Xu, X., 2015. Environment and ecology of East Asian dinosaurs during the Early Cretaceous inferred from stable oxygen and carbon isotopes in apatite. Journal of Asian Earth Sciences 98, 358–370.

Aplin, A.C., Matenaar, I.F., McCarty, D.K., van der Pluijm, B.A., 2006. Influence of Mechanical Compaction and Clay Mineral Diagenesis on the Microfabric and Pore-Scale Properties of Deep-Water Gulf of Mexico Mudstones. Clays and Clay Minerals 54, 500–514.

Baioumy, H.M., 2004. Clay mineralogy of Upper Cretaceous-Lower Tertiary in Egypt and its paleoclimatic implication. Clay Science 12, 223–234.

Berner, R.A., Lasaga, A.C., Garrels, R.M., 1983. The carbonate-silicate geochemical cycle and its effects on atmospheric carbon dioxide over the past 100 million years. American Journal of Science 283, 641–683.

Blenkinsop, T.G., 1988. Definition of low-grade metamorphic zones using illite crystallinity. Journal of Metamorphic Geology 6, 623–636.

Bozkaya, Ö., Yalçın, H., Göncüoglu, M.C., 2011. Diagenetic and very low-grade metamorphic characteristics of the Paleozoic units of the Istanbul Terrane (NW Turkey). In: European Clay Conference-EUROCLAY 2011, 26 June–01 July 2011, (Antalya, Turkey).

Cai, Y., Ouyang, F., Luo, X., Zhang, Z., Wen, M., Luo, X., Tang, R., 2022. Geochemical Characteristics and Constraints on Provenance, Tectonic Setting, and Paleoweathering of Middle Jurassic Zhiluo Formation Sandstones in the Northwest Ordos Basin, North-Central China. Minerals 12, 603. https://doi.org/10.3390/min12050603.

Chamley, H., 1989. Clay sedimentology. Springer Verlag, Berlin, p. 623.

Cho, T., Mantani, H., Ohta, T., Li, G., 2019. Evaluation of Cretaceous Hinterland Weathering and Climate in the Sichuan Basin, SW China. Open Journal of Geology 9, 696–699.

Cho, T., Ohta, T., 2022. A robust chemical weathering index for sediments containing authigenic and biogenic materials. Palaeogeography, Palaeoclimatology, Palaeoecology 608, 111288.

Cifuentes, G.R., Jiménez-Millán, J., Quevedo, C.P., Nieto, F., Cuadros, J., Jiménez-Espinosa, R., 2021. Low Temperature Illitization through Illite-Dioctahedral Vermiculite Mixed Layers in a Tropical Saline Lake Rich in Hydrothermal Fluids (Sochagota Lake, Colombia). Minerals 11 (5), 523.

Curtis, C.D., 1985. Clay mineral precipitation and transformation during burial diagenesis. Philosophical transactions of the Royal Society of London A 315, 91–105.

Das, S.S., Rai, A.K., Akaram, V., Verma, D., Pandey, A.C., Dutta, K., Prasad, G.V.R., 2013. Paleoenvironmental significance of clay mineral assemblages in the southeastern Arabian Sea during last 30 kyr. Journal of Earth System Science 122, 173–185.

Dinis, J., Mendes, M., Rey, M., Pais, J., 2016. Geochemistry and mineralogy of the Lower Cretaceous of the Lusitanian Basin (western Portugal): deciphering palaeoclimates from weathering indices and integrated vegetational data. Comptes Rendus Geoscience 348, 139–149.

Doebelin, N., Kleeberg, R., 2015. Profex: a graphical user interface for the Rietveld refinement program BGMN. Journal of Applied Crystallography 48, 1573–1580.

Fang, X.M., Song, C.H., Yan, M.D., Zan, J.B., Liu, C.L., Sha, J.G., Zhang, W.L., Zeng, Y.Y., Wu, S., Zhang, D.W., 2016. Mesozoic litho- and magneto-stratigraphic evidence from the central Tibetan Plateau for megamonsoon evolution and potential evaporates. Gondwana Research 37, 110–129.

Farnsworth, A., Lunt, D.J., Robinson, S.A., Valdes, P.J., Roberts, W.H., Clift, P.D., Markwick, P., Su, T., Wrobel, N., Bragg, F., Kelland, S.-J., Pancost, R.D., 2019. Past East Asian monsoon evolution controlled by paleogeography, not CO2. Science Advances 5 (10), eaax1697.

Faure, M., Lepvrier, C., Nguyen, V.V., Vu, T.V., Lin, W., Chen, Z., 2014. The South China block-Indochina collision: Where, when, and how? Journal of Asian Earth Sciences 79, 260–274.

Fedo, C.M., Nesbitt, H.W., Young, G.M., 1995. Unraveling the effects of potassium metasomatism in sedimentary rocks and paleosols, with implications for paleoweathering conditions and provenance. Geology 23 (10), 921–924.

Findlay, R.H., Trinh, P.T., 1997. The structural setting of the Song Ma Region, Vietnam, and Indochina plate boundary problem. Gondwana Research 1, 11–13.

Foster, G., Royer, D., Lunt, D., 2017. Future climate forcing potentially without precedent in the last 420 million years. Nature Communications 8, 14845. https://doi.org/10.1038/ncomms14845.

Gu, Z., Huang, B., Chen, C., et al., 1976. Editorial Group on "The Lamellibranch Fossils of China" of Nanjing Institute of Geology and Palaeontology, Academia Sinica]. The Lamellibranch Fossils of China. Science Press, Beijing, p. 522 (In Chinese).

Hadji, F., Marok, A., Samet, A.M., 2019. Miocene sediment mineralogy of the lower Chelif basin (NW Algeria): implication for weathering and provenance. Turkish Journal of Earth Sciences 28, 85–102.

Hall, R., 2002. Cenozoic geological and plate tectonic evolution of SE Asia and the SW Pacific: Computer-based reconstructions, model and animations. Journal of Asian Earth Sciences 20, 353–431.

Harnois, L., 1988. The CIW index: A new chemical index of weathering. Sedimentary Geology 55, 319–322.
Hasegawa, H., Imsamut, S., Charusiri, P., Tada, R., Horiuchi, Y., Hisada, K., 2010. "Thailand was a desert" during the mid-Cretaceous: Equatorward shift of the subtropical high-pressure belt indicated by eolian deposits (Phu Thok Formation) in the Khorat Basin, northern Thailand. Island Arc 19, 605–621.
Hasegawa, H., Tada, R., Jiang, X., Suganuma, Y., Imsamut, S., Charusiri, P., Ichinnorov, N., Khand, Y., 2012. Drastic shrinking of the Hadley circulation during the mid-Cretaceous supergreenhouse. Climate of the Past 8, 1323–1337.
Hay, W.W., Floegel, S., 2012. New thoughts about the Cretaceous climate and oceans. Earth-Science Reviews 115, 262–272.
Herrero, M.J., Escavy, J.I., Schreiber, B.C., 2015. Thenardite after mirabilite deposits as a cool climate indicator in the geological record: lower Miocene of central Spain. Climate of the Past 11, 1–13.
Higuchi, T., Abe-Ouchi, A., Chan, W.-L., 2021. Differences between Present-day and Cretaceous hydrological cycle responses to rising $CO_2$ concentration. Geophysical Research Letters 48, e2021GL094341. https://doi.org/10.1029/2021GL094341.
Hoang, N., Shinjo, R., Phuc, L.T., Anh, L.D., Huong, T.T., Pécskay, Z., Bac, D.T., 2019. Pleistocene basaltic volcanism in the Krông Nô area and vicinity, Dac Nong Province (Vietnam). Journal of Asian Earth Sciences 181, 103903.
Horiuchi, Y., Charusiri, P., Hisada, K., 2012. Identification of an anastomosing river system in the Early Cretaceous Khorat Basin, northeastern Thailand, using stratigraphy and palaeosols. Journal of Asian Earth Sciences 61, 62–77.
Hu, X., Wagreich, M., Yilmaz, I.O., 2012. Marine rapid environmental/climatic change in the Cretaceous greenhouse world. Cretaceous Research 38, 1–6.
Hu, B., Li, J., Cui, R., Wei, H., Zhao, J., Li, G., Fang, X., Ding, X., Zou, L., Bai, F., 2014. Clay mineralogy of the riverine sediments of Hainan Island, South China Sea: Implications for weathering and provenance. Journal of Asian Earth Sciences 96, 84–92.
Huber, B., Norris, R.D., MacLeod, K.G., 2002. Deep-sea paleotemperature record of extreme warmth during the Cretaceous. Geology 30, 123–126.
Hung, D.D., Tsutsumi, Y., Hieu, P.T., Minh, N.T., Minh, P., Dung, N.T., Hung, N.B., Komatsu, T., Hoang, N., Kawaguchi, K., 2022. Van Canh Triassic granite in the Kontum Massif, central Vietnam: Geochemistry, geochronology, and tectonic implications. Journal of Asian Earth Sciences 7, 100075.
Hung, K.T., 2009. Tectonics and Magmatism in Northwest Vietnam. Geologia 35, 345–351.
Huu, L.T., Luc, X.V., 2003. New finding of fauna and flora fossils in red beds at Yen Chau area, Son La province. Vietnam Journal of Geology 279 (in Vietnamese with English abstract).
Huu, L.T., Vinh, N.P., Duong, P.V., 2008. Geological and mineral features of Upper Cretaceous red beds in Yen Chau basin, Son La. Vietnam Journal of Geology 306 (in Vietnamese).
Jiang, X.S., Li, Y.W., 1996. Spatio-temporal distribution of the Cretaceous deserts in central and eastern China and its climatic significance. Sedimentary Facies and Palaeogeography 16, 42–51 (in Chinese).
Jiang, X.S., Pan, Z.X., Fu, Q.P., 2001. Primary study on pattern of general circulation of atmosphere before uplift of the Tibetan Plateau in eastern Asia. Science in China 44 (D), 666–688 (in Chinese with English abstract).
Khien, N.X., 2005. Stratigraphy of Cretaceous non-marine red beds in the North Vietnam. Vietnam Journal of Earth Science 27 (1), 82–88 (in Vietnamese with English abstract).
Khuc, V.D., 2000. Cretaceous environments in Viet Nam, Laos and Cambodia. In: Okada, H., Mateer, J.N. (Eds.), Cretaceous Environments of Asia. Elsevier, pp. 201–206.
Kübler, B., 1968. Evaluation quantitative du métamorphisme par la cristallinité de l'illite. Bull Centre Rech Pau-SNPA 2, 385–397 (in French).
Lanson, B., Sakharov, B.A., Claret, F., Drits, V.A., 2009. Diagenetic smectite-to-illite transition in clay-rich sediments: A reappraisal of X-ray diffraction results using the multi-specimen method. American Journal of Science 309, 476–516.
Li, P., Rui, G., Junwen, C., Ye, G., 2004. Paleomagnetic analysis of eastern Tibet: implications for the collisional and amalgamation history of the Three Rivers Region, SW China. Journal of Asian Earth Sciences 24, 291–310.
Li, X.H., Chen, S.D., Cao, K., Chen, Y.H., Xu, B.L., Ji, Y.N., 2009. Paleosols of the mid-Cretaceous: A report from Zhejiang and Fujian, SE China. Earth Science Frontiers 16 (5), 63–70.
Li, J., Wen, X.Y., Huang, C.M., 2016. Lower Cretaceous paleosols and paleoclimate in Sichuan Basin, China. Cretaceous Research 62, 154–171.
Li, G., Wu, C., Rodríguez-López, J.P., Yi, H., Xia, G., Wagreich, M., 2018. Mid-Cretaceous aeolian desert systems in the Yunlong area of the Lanping Basin, China: Implications for palaeoatmosphere dynamics and paleoclimatic change in East Asia. Sedimentary Geology 364, 121–140. https://doi.org/10.1016/j.sedgeo.2017.12.014.
Li, J., Wen, X., Huang, C., 2018. Lower and upper Cretaceous paleosols in the western Sichuan Basin, China: Implications for regional paleoclimate. Geological Journal 55, 1–19.
Li, M., Sun, S., Yan, M., Meng, F., Fang, X., Song, X., Zhu, L., 2020. Late Cretaceous paleoclimate reconstruction from halite in an evaporite deposit on the Khorat Plateau, Laos. Cretaceous Research 116, 104589.
Limmer, D.R., Köhler, C.M., Hillier, S., Moreton, S.G., Tabrez, A.R., Clift, P.D., 2012. Chemical weathering and provenance evolution of Holocene–Recent sediments from the Western Indus Shelf, Northern Arabian Sea inferred from physical and mineralogical properties. Marine Geology 326–328, 101–115.
Liu, Z., Colin, C., Trentesaux, A., Blamart, D., Bassinot, F., Siani, G., Sicre, M.-A., 2004. Erosional history of the eastern Tibetan Plateau since 190 kyr ago: clay mineralogical and geochemical investigations from the southwestern South China Sea. Marine Geology 209, 1–18.
Liu, Z., Colin, C., Huang, W., Le, P.K., Tong, S., Chen, Z., Trentesaux, A., 2007. Climatic and tectonic controls on weathering in South China and Indochina Peninsula: clay mineralogical and geochemical investigations from the Pearl, Red, and Mekong drainage basins. Geochemistry, Geophysics, Geosystems 8, Q05005. https://doi.org/10.1029/2006GC001490.
Luo, Q.Y., Zhong, N.N., Wang, Y.N., Ma, L., Li, M., 2015. Provenance and paleoweathering reconstruction of the Mesoproterozoic Hongshuizhuang Formation (1.4 Ga), northern North China. International Journal of Earth Sciences 104, 1701–1720.
McCaffrey, M.A., Lazar, B., Holland, H.D., 1987. The evaporation path of seawater and the coprecipitation of Br- and K+ with halite. Journal of Sedimentary Research 57 (5), 928–938.
McLennan, S.M., 1993. Weathering and Global Denudation. The Journal of Geology 101, 295–303.
McLennan, S.M., Hemming, S., McDaniel, D.K., Hanson, G.N., 1993. Geochemical approaches to sedimentation, provenance and tectonics. Geological Society of America Special Paper 284, 21–40.
Metcalfe, I., 1988. Origin and assembly of Southeast Asian continental terranes. In: Audley-Charles, M.G., Hallam, A. (Eds.), Gondwana and Tethys, vol. 37. Geological Society, London, Special Publication, pp. 101–118.
Metcalfe, I., 2002. Permian tectonic framework and palaeogeography of SE Asia. Journal of Asian Earth Sciences 20, 551–566.
Metcalfe, I., 2011. Palaeozoic-Mesozoic history of SE Asia. In: Hall, R., Cottam, M.A., Wilson, M.E.J. (Eds.), The SE Asian Gateway: History and Tectonics of the Australia-Asia Collision, vol. 355. Geological Society, London, Special Publications, pp. 7–35.
Metcalfe, I., 2013. Gondwana dispersion and Asian accretion: Tectonic and palaeogeographic evolution of eastern Tethys. Journal of Asian Earth Sciences 66, 1–33.
Meunier, A., Lanson, B., Beaufort, D., 2000. Vermiculitization of smectite interfaces and illite layer growth as a possible dual model for illite-smectite illitization in diagenetic environments: a synthesis. Clay Minerals 35 (3), 573–586.
Meunier, A., Lanson, B., Velde, B., 2004. Composition variation of illite-vermiculite-smectite mixed-layer minerals in a bentonite bed from Charente (France). Clay Minerals 39, 317–332.
Millot, G., 1970. Geology of Clays. Springer-Verlag, Berlin, Germany, p. 425.
Moore, D.M., Reynolds, J.R.C., 1997. X-ray diffraction and the identification and analysis of clay minerals. Oxford University Press, Oxford, p. 378.
Nesbitt, H.W., Young, G.M., 1982. Early proterozoic climates and plate motions inferred from major element chemistry of lutites. Nature 299, 715–717.
Ohta, T., Arai, H., 2007. Statistical empirical index of chemical weathering in igneous rocks: A new tool for evaluating the degree of weathering. Chemical Geology 240, 280–297.
Ohta, T., Li, G., Hirano, H., Sakai, T., Kozai, Yoshikawa, T., Kaneko, A., 2011. Early Cretaceous Terrestrial Weathering in Northern China: Relationship between Paleoclimate Change and the Phased Evolution of the Jehol Biota. The Journal of Geology 119, 81–96.
Parker, A., 1970. An index of weathering for silicate rocks. Geological Magazine 107, 501–504.
Penman, D.E., Rugenstein, J.K.C., Ibarra, D.E., Winnick, M.J., 2020. Silicate weathering as a feedback and forcing in Earth's climate and carbon cycle. Earth-Science Reviews 209, 103298.
Perri, F., Ohta, T., 2014. Paleoclimatic conditions and paleoweathering processes on Mesozoic continental redbeds from Western-Central Mediterranean Alpine Chains. Palaeogeography, Palaeoclimatology, Palaeoecology 395, 144–157.
Replumaz, A., Tapponnier, P., 2003. Reconstruction of the deformed collision zone between India and Asia by backward motion of lithospheric blocks. Journal of Geophysical Research 108 (B6), 2285. https://doi.org/10.1029/2001JB00066.
Retallack, G.J., 2001. A 300-million-year record of atmospheric carbon dioxide from fossil plant cuticles. Nature 411, 287.
Robert, C., Chamely, H., 1991. Development of early Eocene warm climates, as inferred from clay variations in oceanic sediments. Palaeogeography, Palaeoclimatology, Palaeoecology 89, 315–331.
Roger, F., Maluski, H., Lepvrier, C., Vu, V.T., Paquette, J.L., 2012. LA-ICPMS zircons U/Pb dating of Permo-Triassic and Cretaceous magmatisms in Northern Vietnam-Geodynamical implication. Journal of Asian Earth Sciences 48, 72–82.
Roser, B.P., Korsch, R.J., 1988. Provenance signatures of sandstone-mudstone suites determined using discriminant function analysis of major-element data. Chemical Geology 67, 119–139.
Royer, D.L., Berner, R.A., Beerling, D.J., 2001. Phanerozoic atmospheric CO2 change: evaluating geochemical and paleobiological approaches. Earth-Science Reviews 54, 349–392.
Ruffell, A.H., Price, G.D., Mutterlose, J., Kessels, K., Baraboshkin, E., Gröcke, D.R., 2002. Palaeoclimate indicators (clay minerals, calcareous nannofossils, stable isotopes) compared from two successions in the late Jurassic of the Volga Basin (SE Russia). Geological Journal 37, 17–33.
Sakai, T., Nghinh, L.T., Ngoc, N.T., Khien, N.X., Saka, Y., Hirano, H., Huu, L.T., 2006. Sedimentary facies and depositional systems of the Cretaceous Yen Chau basin, West Bac Bo, Viet Nam. Vietnam Journal of Geology 27.

Sato, K., Liu, Y., Zhu, Z., Yang, Z., Otofuji, Y., 1999. Paleomagnetic studies of middle Cretaceous rocks from Yunlong, western Yunnan, China: evidence of southward displacement of Indochina. Earth and Planetary Science Letters 165, 1–15.

Shi, M.-F., Lin, F.-C., Fan, W.-Y., Deng, Q., Cong, F., Tran, M.-D., Zhu, H.-P., Wang, H., 2015. Zircon U-Pb ages and geochemistry of granitoids in the Truong Son terrane, Vietnam: Tectonic and metallogenic implications. Journal of Asian Earth Sciences 101, 101–120.

Su, C.-M., Wen, S., Tang, C.-C., Yeh, Y.-L., Chen, C.-H., 2018. The variation of crustal structure along the Song Ma Shear Zone, Northern Vietnam. Tectonophysics 734–735, 119–129.

Tabakh, M.E., Utha-Aroon, C., Schreiber, B.C., 1999. Sedimentology of the Cretaceous Maha Sarakham evaporites in the Khorat Plateau of northeastern Thailand. Sedimentary Geology 123, 31–62.

Tabor, C.R., Poulsen, C.J., Lunt, D.J., Rosenbloom, N.A., Otto-Bliesner, B.L., Markwick, P.J., Brady, E.C., Farnsworth, A., Feng, R., 2016. The cause of Late Cretaceous cooling: A multimodel-proxy comparison. Geology 44 (11), 963–966. https://doi.org/10.1130/g38363.1.

Takemoto, K., Halim, N., Otofuji, Y., Tri, T.V., De, L.V., Hada, S., 2005. New paleomagnetic constraints on the extrusion of Indochina: Late Cretaceous results from the Song Da terrane, northern Vietnam. Earth and Planetary Science Letters 229, 273–285.

Taylor, S.R., McLennan, S.M., 1985. The Continental Crust: Its Composition and Evolution. Blackwell Scientific Publications, Blackwell, Oxford, UK, p. 312.

Thamban, M., Rao, V.P., Schneider, R.R., 2002. Reconstruction of late Quaternary monsoon oscillations based on clay mineral proxies using sediment cores from the western margin of India. Marine Geology 186, 527–539.

Thanh, T.D., Khuc, V., 2006. Stratigraphic units of Vietnam. Vietnam National University Publishing House, Hanoi, p. 526.

Thanh, T.V., Hieu, P.T., Minh, P., Nhuan, D.V., Thuy, N.T.B., 2019. Late Permian-Triassic granitic rocks of Vietnam: the Muong Lat example. International Geology Review 61, 1823–1841.

Tian, Z., Tang, W., Wang, P., Zhao, Z., Sun, X., Tang, H., 2021. Tectonic Evolution and Key Geological Issues of the Proto South China Sea. Acta Geologica Sinica 95 (1), 77–90.

Velde, B., Vasseur, G., 1992. Estimation of the diagenetic smectite to illite transformation in time-temperature space. American Mineralogist 77, 967–976.

Velde, B., 1995. Origin and Mineralogy of Clays: Clays and the Environment. Springer-Varlag, New York, NY, USA.

Wagner, T., Hofmann, P., Flögel, S., 2013. Marine black shale deposition and Hadley Cell dynamics: a conceptual framework for the Cretaceous Atlantic Ocean. Marine and Petroleum Geology 43, 222–238.

Walker, J.C.G., Hays, P.B., Kasting, J.F., 1981. A negative feedback mechanism for the long-term stabilization of Earth's surface temperature. Journal of Geophysical Research 86 (C10), 9776–9782. https://doi.org/10.1029/JC086iC10p09776.

Wang, C., Hu, X., Huang, Y., Wagreich, M., Scott, R., Hay, W., 2009. Cretaceous oceanic red beds as possible consequence of oceanic anoxic events. In: Hu, X., Wang, C., Scott, R.W., Wagreich, M., Jansa, L. (Eds.), Cretaceous Oceanic Red Beds: Stratigraphy, Composition, Origins and Paleoceanographic/Paleoclimatic Significance, vol. 91. SEPM Special Publication, Tulsa, OK, pp. 13–33.

Wang, Y., Huang, C., Sun, B., Quan, C., Wu, J., Lin, Z., 2014. Paleo-CO2 variation trends and the Cretaceous greenhouse climate. Earth-Science Reviews 129, 136–147. https://doi.org/10.1016/j.earscirev.2013.11.001.

Wang, S., Mo, Y., Wang, C., Ye, P., 2016. Paleotethyan evolution of the Indochina Block as deduced from granites in northern Laos. Gondwana Research 38, 183–196.

Wang, L., Zhong, Y., Xi, D., Hi, J., Shen, L., Dong, H., Liu, C., Ding, L., 2021. The Middle to Late Cretaceous marine incursion of the Proto-Paratethys Sea and Asian aridification: A case study from the Simao-Khorat salt giant, Southeast Asia. Palaeogeography, Palaeoclimatology, Palaeoecology 567, 110300.

Wang, J.Y., Li, X.H., Li, L.Q., Wang, Y.D., 2022. Cretaceous climate variations indicated by palynoflora in South China. Palaeoworld 31, 507–520.

Wronkiewicz, D.J., Condie, K.C., 1987. Geochemistry of Archean shales from the Witwatersrand Supergroup, South Africa: Source-area weathering and provenance. Geochimica et Cosmochimica Acta 51 (9), 2401–2416.

Wu, G., Yano, T., Tan, M., 2004. Sedimentary facies of the Jingxing Formation of Lower Cretaceous in Lanping Basin, West Yunnan. Journal of Palaeogeography 6, 380–384.

Wu, C., Liu, C., Yi, H., Xia, G., Zhang, H., Wang, L., Li, G., Wagreich, M., 2017. Mid-Cretaceous desert system in the Simao Basin, southwestern China, and its implications for sea-level change during a greenhouse climate. Palaeogeography, Palaeoclimatology, Palaeoecology 468, 529–544.

Xu, G., Deconinck, J.-F., Feng, Q., Baudin, F., Pellenard, P., Shen, J., Bruneau, L., 2017. Clay mineralogical characteristics at the Permian–Triassic Shangsi section and their paleoenvironmental and/or paleoclimatic significance. Palaeogeography, Palaeoclimatology, Palaeoecology 474, 152–163.

Yan, Y., Xia, B., Lin, G., Cui, X., Hu, X., Yan, P., Zhang, F., 2007. Geochemistry of the sedimentary rocks from the Nanxiong Basin, South China and implications for provenance, paleoenvironment and paleoclimate at the K/T boundary. Sedimentary Geology 197, 127–140.

Yan, M., Zhang, D., Fang, X., Zhang, W., Song, C., Liu, C., Zan, J., Shen, M., 2021. New insights on the age of the Mengyejing Formation in the Simao Basin, SE Tethyan domain and its geological implications. Science China Earth Sciences 64 (2), 231–252. https://doi.org/10.1007/s11430-020-9689-3/.

Yang, Z., Besse, J., 1993. Paleomagnetic studies of Permian and Mesozoic sedimentary rocks from Northern Thailand support the extrusion model for Indochina. Earth and Planetary Science Letters 117, 525–552.

Yang, Y.T., 2013. An unrecognized major collision of the Okhotomorsk Block with East Asia during the Late Cretaceous, constraints on the plate reorganization of the Northwest Pacific. Earth-Science Reviews 126, 96–115.

Ye, C., Yang, Y., Fang, X., Guo, Z., Zhang, W., Liu, Y., 2022. Evolution of Paleogene weathering intensity in the Qaidam Basin, northeastern Tibetan Plateau: Insights from clay geochemistry. Catena 213, 106162.

Young, G.M., Nesbitt, H.W., 1998. Processes controlling the distribution of Ti and Al in weathering profiles, siliciclastic sediments and sedimentary rocks. Journal of Sedimentary Research 68 (3), 448–455.

Yu, L., Li, Q., Wang, F., Liu, X., 2014. Petrogenesis and tectonic significance of the Late Cretaceous magmatism in the Northern part of the Baoshan block: constraints from bulk geochemistry, zircon U-Pb geochronology and Hf isotopic compositions. Acta Geologica Sinica 30, 2709–2724.

Zhang, L., Wang, C., Cao, K., Wang, Q., Tan, J., Gao, Y., 2016. High elevation of Jiaolai Basin during the Late Cretaceous: Implication for the coastal mountains along the East Asian margin. Earth and Planetary Science Letters 456, 112–123. https://doi.org/10.1016/j.epsl.2016.09.034.

Zhang, D., Yan, M., Fang, X., Yang, Y., Zhang, T., Zan, J., Zhang, W., Liu, C., Yang, Q., 2018. Magnetostratigraphic study of the potash-bearing strata from drilling core ZK2893 in the Sakhon Nakhon Basin, eastern Khorat Plateau. Palaeogeography, Palaeoclimatology, Palaeoecology 489, 40–51. https://doi.org/10.1016/j.palaeo.2017.08.030.

Zhang, J., Liu, Y., Flögel, S., Zhang, T., Wang, C., Fang, X., 2021a. Altitude of the East Asian Coastal Mountains and Their Influence on Asian Climate During Early Late Cretaceous. Journal of Geophysical Research: Atmospheres 126, e2020JD034413. https://doi.org/10.1029/2020JD034413.

Zhang, J., Liu, Y., Fang, X., Zhang, T., Zhu, C., Wang, C., 2021b. Elevation of the Gangdese Mountains and their impacts on Asian climate during the Late Cretaceous - a modeling study. Frontiers in Earth Science 9, 810931.

Zhang, D., Yan, M., Fang, X., Zhang, W., Shen, M., Song, C., 2025. Cretaceous magnetostratigraphy of the southern Simao Basin, SE Tibetan Plateau, and its paleogeographic implications. Geological Society of America Bulletin 137, 613–629.

Zhu, Z., Zhai, Q., Hu, P., Tang, Y., Wang, H., Wang, W., Wu, H., 2022. Resolving the timing of Lhasa-Qiangtang block collision: Evidence from the Lower Cretaceous Duoni Formation in the Baingoin foreland basin. Palaeogeography, Palaeoclimatology, Palaeoecology 595, 110956.